Journal of Metals, Materials and Minerals, 36(1), e2555, 2026

A review on biomass-derived hard carbon anodes for sodium-ion batteries: From carbon precursors to storage mechanisms

Anqi LU[1,2], and Jiaqian QIN[2,3,*]

[1] *International Graduate Program of Nanoscience & Technology, Chulalongkorn University, Phayathai Road, Pathumwan, Bangkok 10330 Thailand*
[2] *Department of Materials Science/Faculty of Science, Chulalongkorn University, Phayathai Road, Pathumwan, Bangkok 10330 Thailand*
[3] *Center of Excellence in Responsive Wearable Materials, Metallurgy and Materials Science Research Institute (MMRI), Chulalongkorn University,Phayathai Road, Pathumwan, Bangkok 10330 Thailand*

***Corresponding author e-mail**: jiaqian.q@chula.ac.th

Received date:
3 November 2025
Revised date:
23 November 2025
Accepted date:
1 December 2025

Keywords:
Sodium-ion batteries;
Biomass-derived precursors;
Hard carbon;
Energy storage

Abstract

The rapid development of sustainable energy technologies has intensified the demand for cost-effective and high-performance energy storage systems. Sodium-ion batteries (SIBs) are regarded as one of the most promising alternatives to lithium-ion batteries (LIBs) owing to their low cost, abundant sodium resources, and similar electrochemical mechanisms to LIBs. Hard carbon (HC) has attracted significant attention as the predominant anode material for SIBs due to its low cost, structural tunability, and availability from diverse precursors. Nevertheless, challenges remain, including the unclear Na^+ storage mechanism, limited rate capability, and strong dependence on precursor type. This review systematically summarizes recent advances in HC anodes for SIBs, focusing on their structural features and Na^+ storage mechanisms, including intercalation–adsorption, adsorption–intercalation, pore-filling, and combined models. Moreover, the influence of different precursors—agricultural and forestry by-products, marine biomass, and industrial wastes—on the microstructure and electrochemical performance of HC is analyzed. Finally, the advantages, limitations, and potential strategies for the rational design of HC are discussed, highlighting opportunities for the development of next-generation SIBs.

1. Introduction

Energy is inextricably linked to human life, and global energy demand has been rising continuously since the Industrial Revolution [1]. Conventional energy sources, such as natural gas, fossil fuels, and coal, remain the dominant contributors. However, the excessive consumption of these non-renewable resources has led to severe ecological degradation and the looming threat of energy depletion [2]. Consequently, energy has become one of the most critical barriers to sustainable global development. In the context of global "carbon neutrality" targets, the establishment of new energy systems is imperative, with renewable and clean alternatives—including solar, nuclear, wind, and hydrogen energy—expected to gradually replace fossil fuels [3]. Nevertheless, despite their promise, these renewable energy sources face intrinsic challenges such as intermittent supply, operational variability, and geographical dependence [4]. Therefore, the development of advanced, large-scale, and sustainable energy storage technologies has become critically important.

Among energy storage technologies, secondary batteries play a pivotal role. Lithium-ion batteries (LIBs), in particular, dominate the market owing to their high energy density, high efficiency, relatively high operating voltage, long cycle life, and negligible memory effect [5]; they are widely applied in portable electronics (e.g., laptops and smartphones) and electric vehicles. However, the rapid growth of electric vehicle markets has drastically increased the demand for lithium resources. The natural abundance of lithium is limited to only 0.0065% of the Earth's crust [7], and its distribution is highly uneven, with most reserves concentrated in South America [8]. As a result, the long-term development of LIBs is hindered by escalating costs, resource scarcity, and restricted potential for large-scale energy storage applications.

To address these limitations, researchers have turned their attention to sodium-ion batteries (SIBs). Sodium, located in the same group as lithium in the periodic table, shares similar physical and chemical properties [9]. More importantly, sodium is abundantly available, comprising about 2.83% of the Earth's crust [10], which is 435 time greater than lithium reserves. Consequently, SIBs have attracted significant attention as an environmentally friendly alternative to LIBs [11]. In fact, the "EU Energy Storage Plan" identifies SIBs as a leading candidate in the secondary battery field, second only to LIBs. Nevertheless, the commercialization of SIBs has been relatively slow, largely due to the lack of suitable anode materials [12]. Since electrode materials are fundamental to energy storage and conversion, directly influence cost and performance, the design of efficient anode materials is crucial for advancing SIB technology.

To date, several types of anode materials have been investigated for SIBs, including alloy-based [13], conversion-based [14], and insertion materials [15]. Alloy-type anodes, composed of elements such as Bi, Sb, Sn, Ge, Pb, P, and Si, can form alloys with sodium [16]. These materials often exhibit high theoretical capacities and

operate around 1.0 V (vs. Na/Na^+), as each metal atom can combine with multiple sodium atoms [17]. Despite these advantages, alloy-type anodes suffer from severe volume expansion during charge–discharge cycles, which compromises structural integrity and cycle stability. The result leads to electrode pulverization, repeated solid–electrolyte interphase (SEI) formation, and rapid capacity fading [17, 18]. Conversion-type materials—including transition metal oxides [14], transition metal sulfides [19], transition metal phosphides [20], and transition metal selenides [21]—store Na^+ through conversion reactions and offer high theoretical specific capacities. However, they face similar challenges, such as large volume changes, sluggish Na^+ diffusion kinetics, and poor cycling stability [22].

In contrast, insertion-type materials—typically titanium-based compounds [23] and carbon-based components [15]—allow reversible Na^+ insertion/extraction. They are generally low-cost, structurally stable, and exhibit good cycling performance at low operating voltages. Carbon-based materials are especially promising because they can take on many different shapes, have tunable microstructures, are very conductive, and are chemically stable [24]. Biomass-derived hard carbon (HC), in particular, offers additional benefits such as low cost, abundant raw materials, simple synthesis routes, and environmental sustainability, making it a highly attractive candidate for SIB anodes [25].

Nevertheless, despite these advantages, biomass-derived HC still faces several challenges. These include poor rate capability, low initial Coulombic efficiency (ICE) [26], and an unclear sodium-storage mechanism [27]. Although many studies have attempted to elucidate the Na^+ storage behavior of HC, debates remain regarding the mechanisms at different voltage ranges [28]. Moreover, the precursor plays a decisive role in determining the electrochemical properties of the final HC product. Biomass precursors derived from various sources exhibit distinct pore structures, compositions, and heteroatom content (e.g., oxygen, nitrogen, sulfur, and phosphorus) [29]. Therefore, effective utilization and recycling of waste biomass for HC production is essential not only for energy storage applications but also for advancing societal sustainability.

In this review, we aim to provide a comprehensive overview of biomass-derived HC anodes for SIBs. Specifically, we: (1) examine and compare the structures and properties of graphite, soft carbon, and HC; (2) analyze and contrast different sodium-storage models proposed for HC, including the intercalation–adsorption, adsorption–intercalation, adsorption–pore filling, and hybrid models; and (3) summarize the influence of various biomass precursors, including agricultural and forestry byproducts, marine-derived sources, and industrial wastes, on HC performance. By consolidating these perspectives, this review seeks to offer theoretical guidance for understanding sodium-storage mechanisms in HC and give suggestions for the rational design of high-performance, biomass-derived HC anodes for next-generation SIBs.

2. The structure and the mechanism of hard carbon

2.1 Structure of carbon-based materials

Carbon is a historically and technologically important element, widely employed in energy storage systems due to its cost-effectiveness, high conductivity, and stable electrochemical properties [30]. Carbon materials can be classified according to their crystallinity and structural dimensions, which are closely related to their electrochemical behavior. Based on crystallinity, carbon materials are generally divided into amorphous carbon [31], turbostratic carbon, and graphitic carbon [32], as shown in Figure 1(a–c). Amorphous carbon exhibits highly disordered atomic arrangements with abundant defects and random pore structures. Turbostratic carbon consists of short-range ordered graphene layers, while adjacent layers are randomly rotated and misaligned without long-range stacking registry. Graphitic carbon, in contrast, is composed of well-aligned sp^2 layers with high crystallinity and long-range order. These structural differences critically influence electronic conductivity, interlayer spacing, ion diffusion, and charge storage behavior [30]. These classification schemes provide a comprehensive framework for understanding the structure–electrochemical performance relationships of different carbon anode materials in SIBs.

Carbon materials can also be classified according to their structural dimensionality, including zero-dimensional (0D, e.g., carbon dots and nanospheres), one-dimensional (1D, e.g., carbon nanotubes and nanofibers), two-dimensional (2D, e.g., graphene and graphene nanosheets), and three-dimensional (3D, e.g., porous carbon frameworks and aerogels) architectures (Figure 1(d-f)) [33]. Dimensionality affects electron and ion transport pathways, surface area, and pore network connectivity, which are essential for optimizing electrochemical performance. For example, 1D and 2D carbons facilitate rapid electron transport along extended networks, whereas 3D porous carbons provide interconnected ion diffusion channels and abundant electrolyte-accessible active sites [34].

Among various carbon materials, graphite, soft carbon, and HC are the most representative anode materials for the batteries. Since the commercialization of LIBs with graphite anodes in 1991, graphite has remained the most prevalent anode material due to its uniform interlayer spacing (0.335 nm) and ability to form LiC_6, with a theoretical capacity of 372 $mAh{\cdot}g^{-1}$ (Figure 2(c)) [35]. In comparison, Figure 2(a) highlights the structural similarity between LIBs and SIBs, as lithium and sodium exhibit comparable physicochemical and electrochemical properties [9]. However, Na^+ intercalation into graphite is limited. The NaC_{64} compound exhibits a low capacity (~34.9 $mAh{\cdot}g^{-1}$), due to the larger ionic radius of Na^+ (0.102 nm) compared to Li^+ (0.076 nm) (Figure 2(b)), which hinders intercalation and renders Na–graphite intercalation compounds thermodynamically unstable [36-38]. Soft carbon is a non-graphitic carbon material whose microstructure typically consists of turbostratic graphene layers. It can be partially graphitized under high-temperature treatment. Although the enlarged interlayer spacing compared with graphite allows limited Na^+ insertion, soft carbon generally exhibits moderate reversible capacity and lower cycling stability in SIBs (Figure 2d).

In contrast, HC (non-graphitizable carbon) contains turbostratic microdomains embedded in a highly disordered amorphous matrix and cannot be graphitized even at high temperatures (Figure 2(e)) [39]. The combination of short-range ordered domains and disordered regions with abundant defects and nanopores provides multiple sodium storage sites, including adsorption, intercalation, and pore-filling [39]. Consequently, HC exhibits higher reversible capacity (~300 $mAh{\cdot}g^{-1}$), low sodium storage potential, good cycling stability, and compatibility with diverse low-cost precursors, making it the most promising anode material for SIBs.

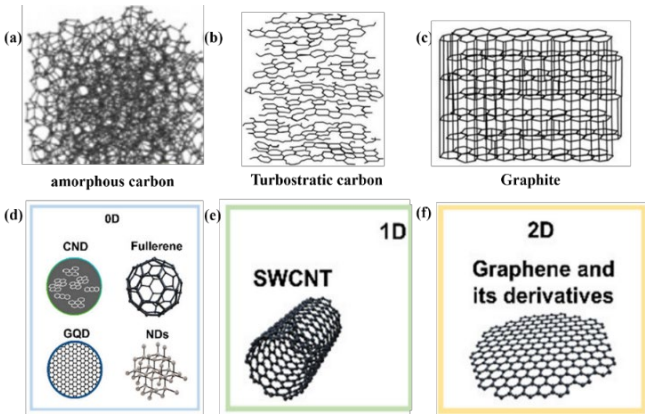

Figure 1. The carbon materials structure of (a) amorphous carbon (Reproduced with permission from ref. [31]. Copyright 2015, ACS), (b) turbostratic carbon, (c) graphite (Reproduced with permission from ref. [32]. Copyright 2023, Wiley-VCH GmbH), and (d-f) the structure of carbon materials of different dimensions (Reproduced with permission from ref. [33]. Copyright 2021, ACS).

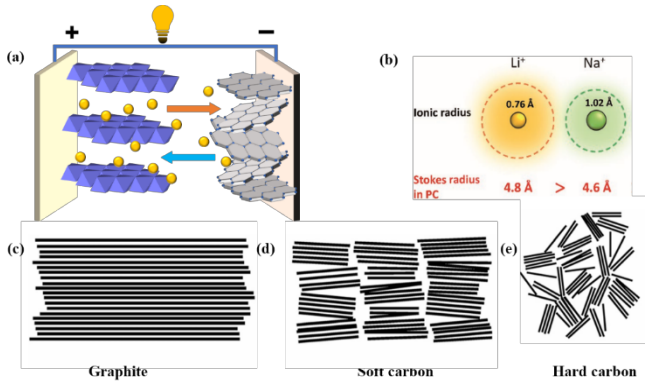

Figure 2. (a) The structure of SIBs, (b) The difference of ionic radius between Li^+ and Na^+ (Reproduced with permission from ref. [37]. Copyright 2022, Royal Society of Chemistry), (c) graphite, (d) soft carbon, and (e) HC (Reproduced from ref. [3]).

Recent studies indicate that Na^+ storage in HC occurs at three distinct sites—surface active sites, interlayer galleries, and nanopores—corresponding to several proposed storage models [28,40]. The electrochemical profile of HC typically features a sloping region above 0.1 V and a plateau region below 0.1 V. While significant progress has been made in elucidating Na^+–HC interactions, the correlation between these voltage regions and specific storage mechanisms remains under debate [41]. Several mechanistic models have been proposed to describe these storage behaviors, which will be discussed in detail in the following sections [40]. Therefore, elucidating the Na^+ storage mechanism in HC is critical for the rational design of high-performance anodes.

2.2 Intercalation-adsorption model

Research into the Na^+ storage mechanism of HC began in 2000. Stevens and Dahn [42] investigated glucose-derived carbon and reported that its Li^+ and Na^+ storage behavior exhibited similar charge–discharge curves. Based on in situ X-ray scattering, they proposed that Na^+ storage in HC resembles Li^+ storage in other carbon materials, which they termed the "intercalation–adsorption" model. According to this model, Na^+ first intercalates into parallel carbon layers, corresponding to the sloping region of the discharge curve, and subsequently adsorbs into nanopores, accounting for the plateau region. To illustrate this behavior, they introduced the "house-of-cards" model, in which some graphene sheets form ordered microcrystalline domains, while others are randomly stacked to create nanoporous structures.

Later, Komaba *et al.* [43] further validated this model using in situ XRD. Their results showed that, upon discharging to 0.2 V, the XRD peak shifted to lower angles, indicating Na^+ insertion into the interlayer space and subsequent expansion (Figure 3(a)). Raman spectroscopy also confirmed that the reversible insertion/extraction of Na^+ within carbon layers dominates the sloping region of the curve (Figure 3(b)). Meanwhile, small-angle X-ray scattering revealed changes in electron density within micropores at voltages below 0.1 V, suggesting Na^+ adsorption and desorption in these regions (Figure 3(c)). Together, these findings provide strong evidence that both intercalation and adsorption occur simultaneously around 0.1 V to ~0.2 V, supporting the intercalation–adsorption model.

However, this model does not fully explain all experimental results. For example, when HC is synthesized from the same precursor at different pyrolysis temperatures, notable discrepancies appear. Low-temperature pyrolysis produces HC with abundant micropores but little or no low-potential plateau. In contrast, higher-temperature pyrolysis reduces micropore volume but enhances capacity in the low-potential region [44], which contradicts the intercalation–adsorption mechanism. Thus, while this model accounts for many observations, further investigation is necessary to clarify the fundamental Na^+.

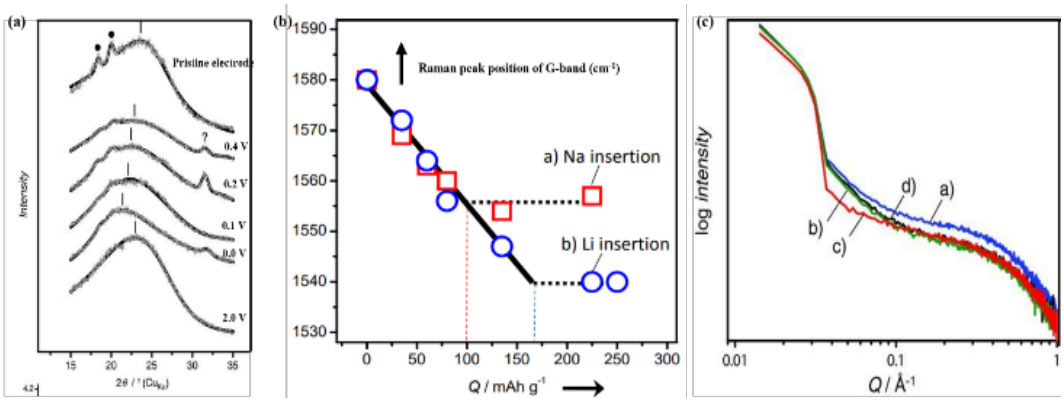

Figure 3. (a) Ex-situ XRD patterns for HC electrodes, (b) Relation between G-band peak position Raman spectrum and capacity for HC electrode, and (c) Ex-situ SAXS patterns for HC electrodes (Reproduced with permission from ref. [43], Copyright 2011 John Wiley and Sons).

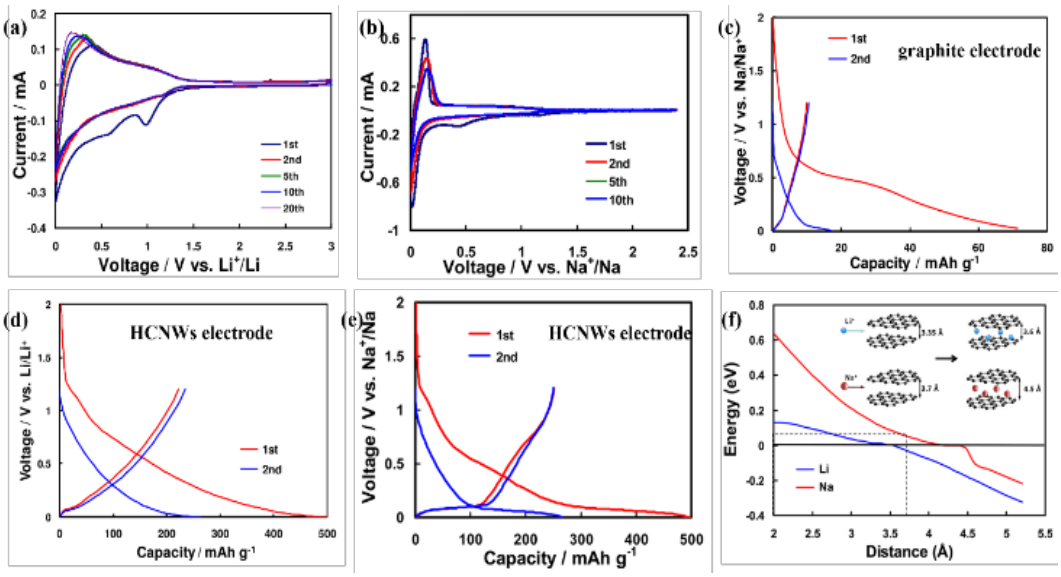

Figure 4. The CV curves of (a) LIBs, (b) SIBs with the HCNW electrode, (c) The GCD curves of SIBs with the graphite electrode, the GCD curves of (d) LIBs, (e) SIBs with the HCNWs electrode, and (f) theoretical energy required for the insertion of Li^+ and Na^+ into carbon (Reproduced with permission from ref. [45]. Copyright 2012, ACS).

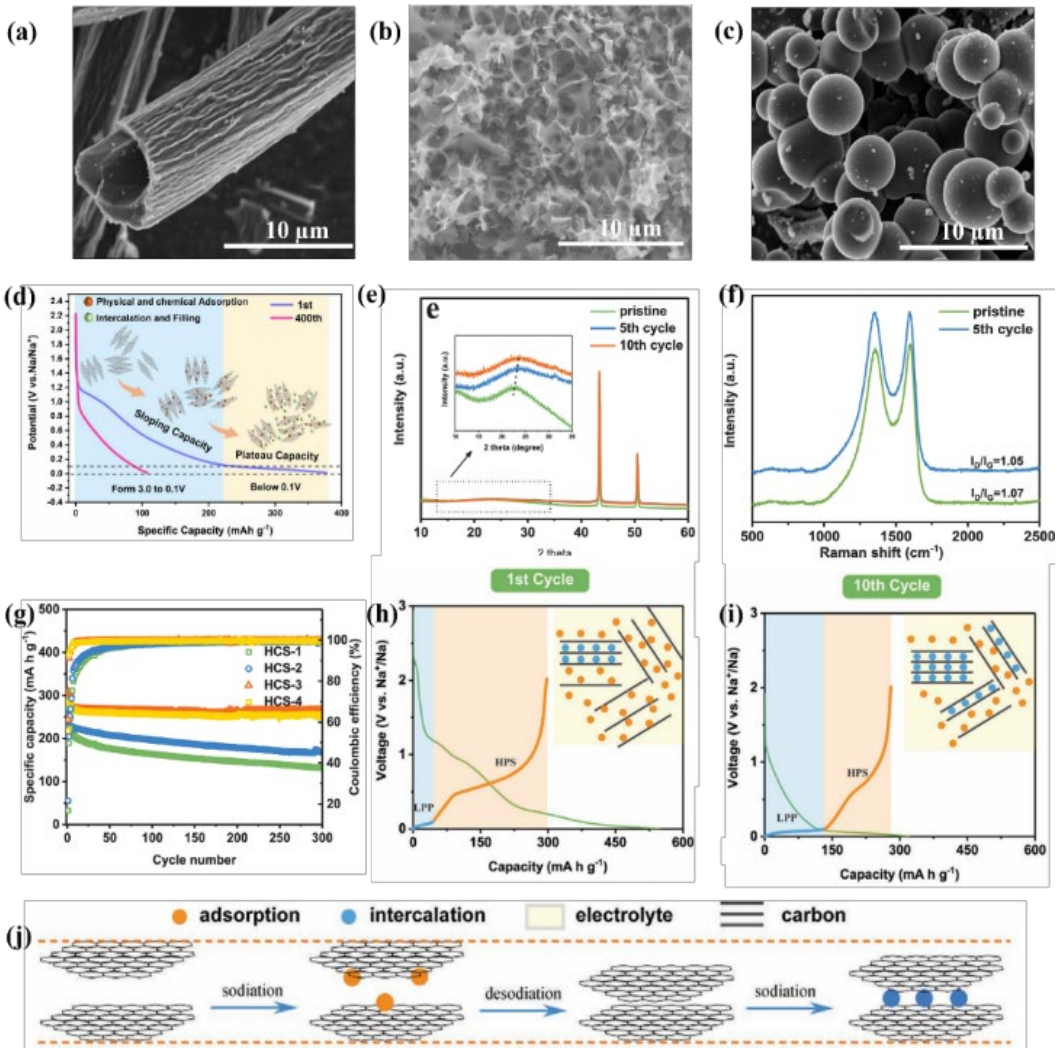

Figure 5. (a-c) The SEM images of HC fibers with different shapes, (d) The mechanism of sodium-ion storage (Reproduced from ref. [46]), (e) XRD pattern, (f) Raman spectrum of HCS-3, (g) cycling performance of the HCS electrode, and (h-j) the mechanism of HCS electrodes during cycles (Reproduced with permission from ref. [47]. Copyright 2021, John Wiley and Sons).

2.3 Adsorption-intercalation model

The adsorption–intercalation model was first proposed by Cao *et al.* [45] in 2012. They synthesized hollow carbon nanowires (HCNWs) by thermally treating polyaniline and investigated their sodium and lithium storage mechanisms, comparing them with the lithium storage behavior of graphite. Their study revealed that HCNWs exhibited markedly different electrochemical responses toward sodium and lithium (Figure 4(a-b)). In the low-potential region, the Na^+ storage mechanism in HCNWs closely resembled that of Li^+ in graphite (Figure 4(c-e)).

To better describe this behavior, they proposed a model in which the sloping region of the discharge curve (>0.2 V) corresponds to Na^+ adsorption on the carbon surface, while the plateau region (<0.2 V) reflects Na^+ intercalation between carbon layers. Theoretical simulations (Figure 4(f)) indicated that the interlayer spacing for Na^+ and Li^+ insertion in HCNWs was 0.450 nm and 0.370 nm, respectively, with corresponding insertion energies of 0.12 eV and 0.03 eV. Because the insertion barrier for Na^+ greatly exceeds the thermal fluctuation energy at room temperature (0.0257 eV), intercalation becomes challenging. However, increasing the interlayer distance significantly lowers the barrier; at 0.370 nm, the insertion energy drops to 0.053 eV, making Na^+ insertion feasible, thus supporting the proposed model.

Later, Yuan *et al.* [46] prepared three morphologies of hydrothermal-derived HC fibers—tubular (TSFC), sheet-like (SSFC), and granular (GSFC)—to evaluate how structural differences affect electrochemical properties (Figure 5(a-c)). TSFC, with its expanded interlayer spacing (0.37 nm) and porous structure, exhibited enhanced electrochemical performance. The discharge curves of TSFC over multiple cycles were consistent with the adsorption–intercalation mechanism (Figure 5(d)).

Chen *et al.* [47] further studied hollow carbon spheres (HCS) with different shell thicknesses. Structural changes during cycling were investigated by XRD and Raman spectroscopy, showing that interlayer spacing contracted and expanded dynamically during charge–discharge (Figure 5(e-f)). They also found that as HCS shell thickness increased, both the defect density and pore volume decreased, leading to lower capacity. Conversely, thinner shells promoted defect-rich surfaces and larger interlayer spacing, consistent with Na^+ adsorption and intercalation behavior (Figure 5(g-j)).

2.4 Adsorption-pore filling model

Li *et al.* [48] reported that the interlayer spacing of HC remained unchanged before and after cycling, as confirmed by XRD and XPS. This suggested that Na^+ was not intercalated into the carbon layers. Instead, they proposed the "adsorption–pore filling" mechanism, in which the sloping region of the charge–discharge curve corresponds to Na^+ adsorption at surface defects, while the low-potential plateau reflects Na^+ storage in micropores.

Bai *et al.* [49] provided additional evidence by incorporating sulfur into HC micropores. After sulfur filling, the plateau below 0.1 V disappeared, while new redox peaks appeared at 1.3 V and 1.6 V (Figure 6(a-b)), confirming that Na^+ occupation of micropores contributes to the plateau capacity. Moreover, higher pyrolysis temperatures reduced defect density, leading to diminished slope capacity (Figure 6(d) and Figure 6(f)). Even when tested with different electrolytes (ether- and ester-based), HC exhibited similar electrochemical behavior. Raman and XRD showed no significant peak shifts (Figure 6(c) and Figure 6(e)), further supporting the conclusion that Na^+ does not intercalate into graphene layers but rather undergoes adsorption and pore-filling processes (Figure 6(g)).

2.5 Adsorption intercalation pore-filling model

The adsorption–intercalation–pore filling model has become the most widely accepted explanation of Na^+ storage in HC. Bommier *et al.* [50] first proposed this model based on studies of sucrose-derived HC. They found that slope capacity correlates strongly with defect concentration (Figures 7(a-b)). Galvanostatic intermittent titration technique (GITT) analysis (Figure 7(c)) revealed higher Na^+ diffusion coefficients in the sloping region than in the plateau region, suggesting that rapid Na^+ adsorption occurs at surface defects, whereas intercalation into carbon layers is hindered by stronger electrostatic repulsion. The XRD result further showed that the interlayer spacing undergoes reversible expansion and contraction between 0.2 V and 0.01 V (Figures 7(d-e)), confirming intercalation at low voltages. Based on these observations, the three-step sodium storage mechanism was proposed: (1) adsorption at defect sites (sloping region), (2) intercalation into graphene layers (plateau), and (3) pore filling in closed nanopores (Figure 7(f)).

Li *et al.* [51] expanded this framework using large-scale molecular dynamics simulations with reactive force fields, demonstrating that sodium adsorption, intercalation, and pore filling jointly account for HC capacity (Figure 7(g-h)). They further showed that slope capacity is closely linked to defect density, while nanopore volume strongly influences plateau capacity.

Reynolds *et al.* [52] confirmed this model experimentally through in situ small-angle neutron scattering (SANS). They observed three distinct steps in commercial HC electrodes: surface adsorption with SEI formation, intercalation into graphene layers, and nanopore filling. Similarly, Chen *et al.* [53] prepared B/P co-doped HC microspheres and found that Na^+ diffusion rates varied across potential regions: rapid adsorption at high voltages (>0.10 V), followed by slower intercalation and pore filling below 0.10 V, consistent with the tripartite model. Raman and XRD also revealed shifts in the G band and d-spacing at low voltages, further validating intercalation and pore-filling contributions.

2.6 Sodium storage in hard carbon: model applicability

Importantly, the precursor type and carbonization conditions play a decisive role in tailoring the microstructure of HC, thereby modulating its dominant sodium storage pathways. Variations in precursor composition and thermal treatment directly influence defect density, interlayer spacing, and pore architecture, leading to different Na^+ storage behaviors. Therefore, establishing clearer correlations between precursor selection, microstructural evolution, and sodium storage mechanisms is essential for resolving the ongoing debate on model applicability and for rationally optimizing HC anodes for SIBs.

2.6.1 Mechanistic summary and model applicability

As summarized in Table 1, the intercalation–adsorption model proposes that Na^+ first intercalates between graphitic layers in the sloping voltage region and subsequently fills closed nanopores in the low-voltage plateau region, emphasizing the critical role of pore structure in determining plateau capacity. In contrast, the adsorption–intercalation model suggests that Na^+ adsorption at defects and edges dominates the high-voltage region, followed by interlayer intercalation at lower potentials, and is more frequently observed in defect-rich HC. Another viewpoint, the adsorption–pore filling model, attributes Na^+ storage mainly to defect adsorption and direct filling of closed nanopores, which is commonly reported for highly disordered or amorphous HC. More recently, the adsorption–intercalation–pore filling model integrates these processes and correlates distinct sodium storage mechanisms with different voltage regions, providing a more comprehensive description of the overall Na^+ storage behavior. Overall, the sodium storage behavior of HC is strongly governed by its microstructural features. Na^+ storage is generally associated with three main types of sites: (1) defect/edge sites, (2) interlayer galleries, and (3) closed nanopores. However, it should be emphasized that no single model can be universally applied to all types of HC. The apparent discrepancies among these models largely stem from the significant structural diversity of HC materials derived from different precursors and carbonization pathways [55]. For instance, highly disordered biomass-derived HCs tend to exhibit dominant defect adsorption and pore-filling behavior, whereas HCs with relatively enlarged interlayer spacing and higher structural ordering may show clearer intercalation features [56]. Consequently, the applicability of a given sodium storage model is strongly dependent on the specific microstructural characteristics of the HC, including defect density, degree of graphitization, interlayer spacing, and pore structure. This structural dependence highlights the necessity of evaluating sodium storage mechanisms in conjunction with detailed microstructural analysis rather than relying on a single universal model.

2.6.2 Challenges and future outlook

Despite extensive investigations, a unified description of Na^+ storage mechanisms in HC has not yet been fully established, primarily due to the structural complexity and diversity introduced by different precursors and carbonization conditions. This structural heterogeneity gives rise to varying contributions from defect sites, interlayer galleries, and closed nanopores, which limits the universal applicability of any single model.

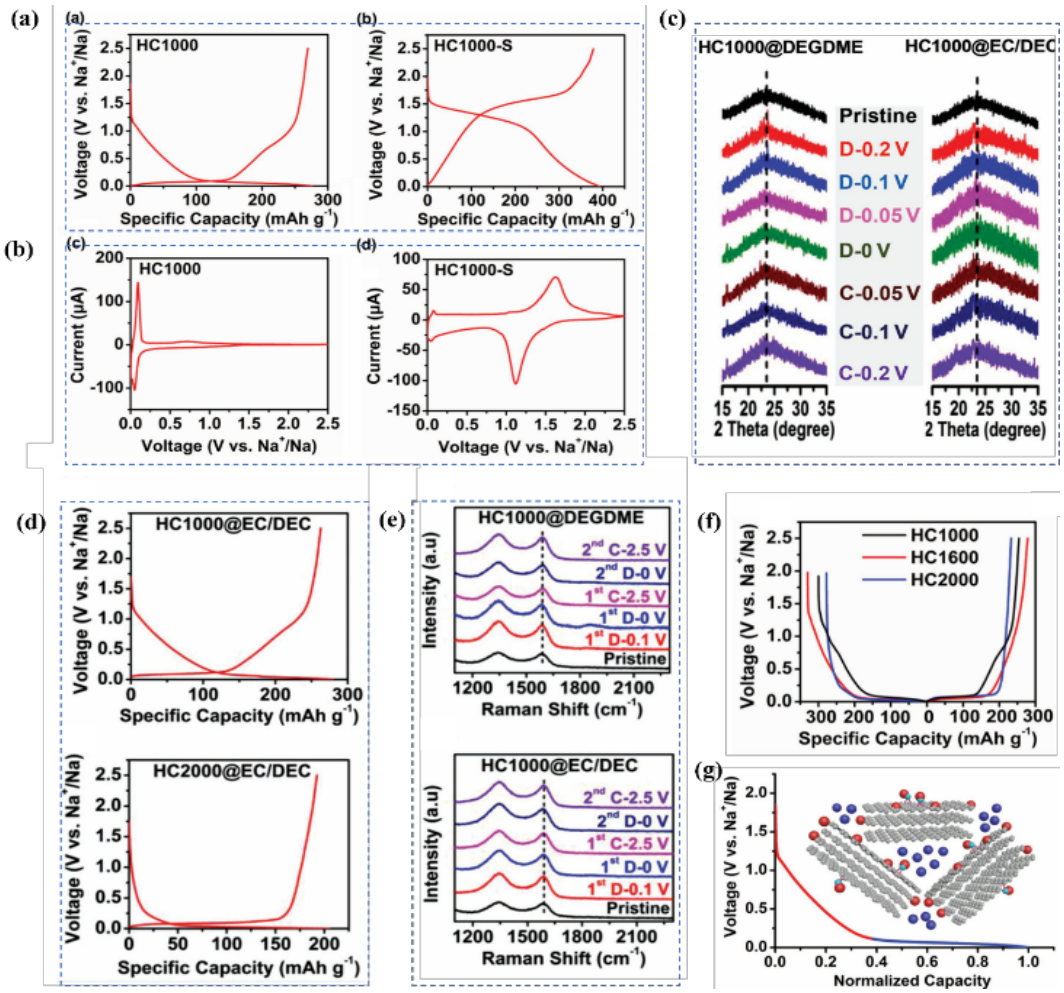

Figure 6. (a) The GCD curves and (b) CV curves of HC and HCs, (c) XRD pattern of HC-1000 at different electrolytes, (d) and (f) The GCD curves of HC at varying temperatures, (e) Raman spectra and (g) the mechanism of HC (Reproduced with permission from ref. [49]. Copyright 2018, John Wiley and Sons).

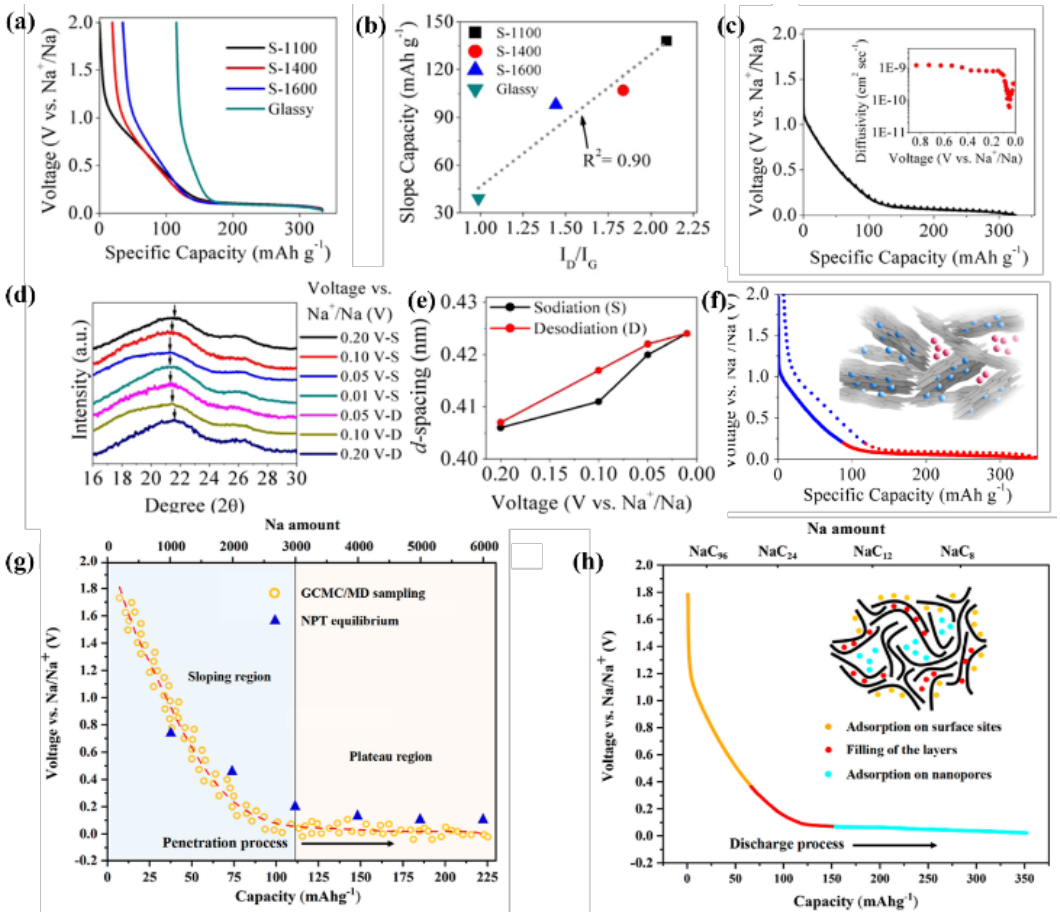

Figure 7. (a) The GCD curves of HC with different pyrolysis temperatures, (b) The correlation between slope capacity and ID/IG, (c) GITT testing, (d) XRD pattern of different voltage, (e) d-spacing of different voltage, (f) The mechanism of HC materials (Reproduced with permission from ref. [50]. Copyright 2015, ACS), (g) Simulated discharge curve for HC models, and (h) Three stages of during discharge curves (Reproduced with permission from ref. [51]. Copyright 2022, ACS).

Table 1. Comparison of Na^+ storage models in HC materials.

Model name	Mechanisms	Features	References
Intercalation-adsorption	(1) Na^+ intercalates into carbon layers at higher voltages; (2) Na^+ adsorbs into pores at low voltages.	Closed pores are crucial for high plateau capacity.	[42,43]
Adsorption-Intercalation	(1) Na^+ adsorbs at defects/edges at higher voltages; (2) Na^+ intercalates between carbon layers at low voltages.	Favored in defect-rich carbons.	[45-47]
Adsorption-pore filling	(1) Na^+ adsorbs at defects/edges; (2) Na^+ directly fills closed pores.	Common in highly amorphous HCs.	[48,49]
Adsorption intercalation pore-filling model	(1) Adsorption at defects (slope region); (2) intercalation between layers (plateau); (3) nanopore filling at very low voltages.	Each stage corresponds to distinct potential regions.	[50-54]

To address these challenges, future studies should focus on establishing more explicit correlations between microstructural parameters and sodium storage pathways using advanced characterization techniques. In particular, synchrotron radiation–based methods, such as operando X-ray diffraction and X-ray absorption spectroscopy, can provide real-time insights into structural evolution and Na^+–carbon interactions during cycling [56]. Complementary in situ/operando spectroscopic techniques, including Raman and nuclear magnetic resonance (NMR) [41], are also essential for elucidating changes in local bonding environments and Na^+ dynamics. Furthermore, integrating these experimental approaches with multiscale modeling and simulation will help quantify the contributions of different storage sites and clarify the applicability of existing models across different HC systems. Such systematic efforts are expected to establish a more transferable mechanistic framework and ultimately guide the rational design of high-performance HC anodes for SIBs.

3. The sources of HC

3.1 The fabrication process

Biomass-derived HC typically exhibits a random structure, enlarged interlayer spacing, and enclosed nanodomains. These structural characteristics make it a promising anode material for SIBs, as it can

provide a high reversible capacity, a relatively low sodium storage potential, and abundant carbon precursors readily available in nature [57]. The predominant preparation strategies for biomass HC include high-temperature pyrolytic carbonization [58], templating methods [59] (hard templating, soft templating, and salt templating), aerogel and emulsion-assisted methods, as well as physical and chemical activation approaches, as shown in Figure 8(a). Regardless of the specific method employed, the synthesis process generally comprises three main stages: pretreatment of raw materials, high-temperature carbonization, and post-treatment [60] (Figure 8(b)). Pretreatment often involves pre-carbonization, acid washing, or alkali washing to remove minerals, inorganic salts, and other impurities that may hinder electrochemical performance [61]. During carbonization, the pretreated biomass is heated in an inert atmosphere (typically argon or nitrogen) at temperatures ranging from 700°C to 1400°C [46]. Post-treatment mainly involves grinding, sieving, and sometimes surface functionalization, with the goal of reducing particle size, introducing additional porosity, or enhancing conductivity to optimize electrochemical behavior.

Biomass is composed mainly of carbon, hydrogen, and oxygen, with minor elements such as sulfur, sodium, potassium, nitrogen, and phosphorus [29]. The intrinsic microstructure and chemical composition of different biomass precursors play a crucial role in shaping the final morphology of HC. Factors such as cellulose-to-lignin ratio, mineral content, and inherent porosity strongly influence the degree of graphitization, pore structure, and surface chemistry of the resulting carbon material [7,62,63]. As a result, HC obtained from various precursors demonstrates significant variability in sodium storage performance, including specific capacity, ICE, and rate capability.

In recent years, in addition to conventional pyrolysis, researchers have explored alternative low-energy and green synthesis approaches, such as hydrothermal carbonization [64], microwave-assisted pyrolysis [65], and molten-salt carbonization [66]. Hydrothermal carbonization, in particular, has attracted attention due to its relatively low operating temperature and its ability to retain oxygen- and nitrogen-rich surface functional groups, which may act as additional sodium adsorption sites [67]. Molten salt synthesis, on the other hand, provides an effective route to control pore formation and interlayer spacing, while microwave-assisted techniques offer fast, energy-efficient heating that may facilitate scalable production [68]. Despite these advances, a major challenge remains in balancing high porosity (for enhanced ion transport) with controlled surface area (to avoid low ICE and unstable SEI formation).

Overall, the fabrication of biomass-derived HC is not merely a matter of thermal decomposition but rather a structure–performance tailoring process in which precursor selection, processing parameters, and post-treatment must be carefully optimized. Continued innovation in synthesis strategies, especially those emphasizing sustainability and energy efficiency, will be vital for advancing biomass HC as a competitive anode candidate for next-generation SIBs.

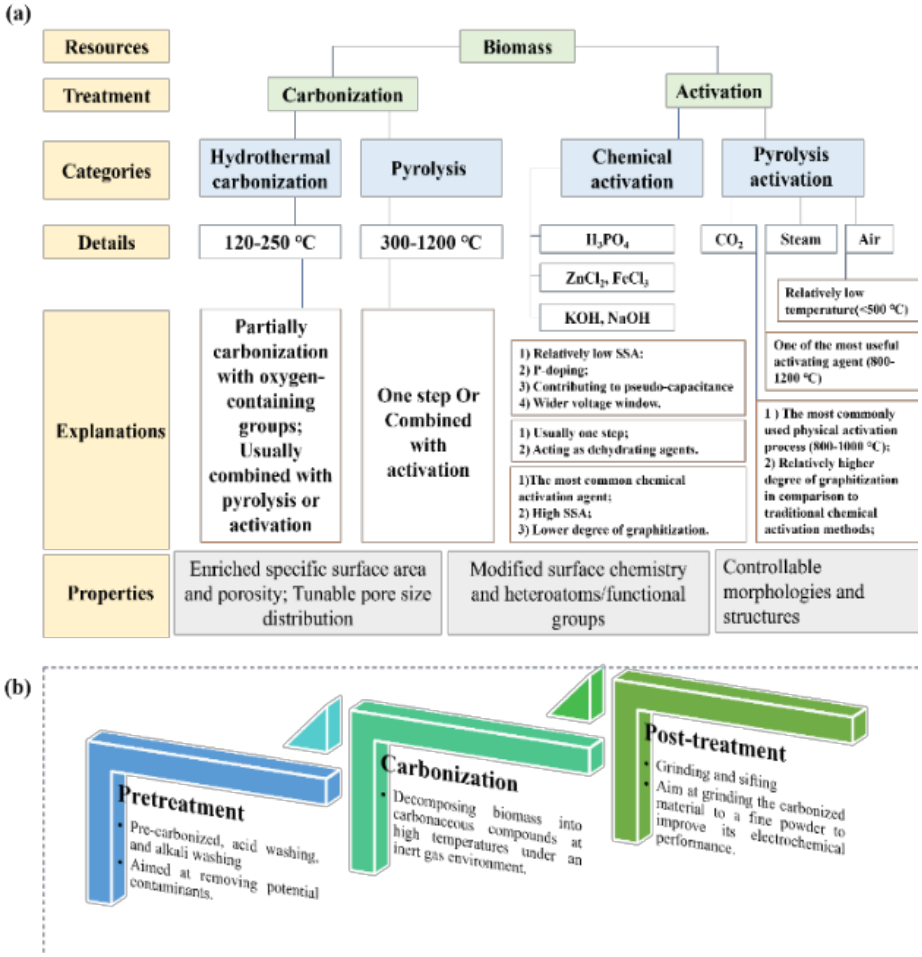

Figure 8. (a) The methods of preparing the biomass HC materials (Content adapted from [57]), and (b) The main steps of preparing the HC materials.

3.2 Agricultural and forestry byproducts

Agricultural and forestry by-products are the most abundant and geographically widespread biomass resources, making them highly cost-effective and attractive precursors for HC synthesis. Common examples include rice husks [62], corn cobs [69], wood chips [1], fruit pits [70], and coconut shells [54]. The structural complexity of these biomasses originates from their major organic components—cellulose, hemicellulose, and lignin—which exist in varying ratios depending on the plant species [71]. The proportion of these components not only determines the physicochemical behavior of the precursor during carbonization but also influences the morphology, porosity, and degree of graphitization of the final HC material [72].

For instance, Tang *et al.* [73] prepared corncob-derived HC via controlled pyrolysis, which exhibited an expanded interlayer spacing (0.376 nm) conducive to Na^+ insertion (Figure 9(a)). The optimized sample (CDHC-1300) delivered a reversible capacity of ~311 mAh·g^{-1} with an initial Coulombic efficiency of ~80%, while retaining ~250 mAh·g^{-1} after 100 cycles, along with excellent rate performance (Figure 9(b)), highlighting the promise of biomass-derived HC as a sustainable anode material for sodium-ion batteries. Zhou *et al.* [74] developed a bamboo-derived HC via stepwise pyrolysis, achieving a high initial Coulombic efficiency of 92.4% and excellent cycling stability, with a reversible capacity of 265.6 mAh·g^{-1} after 500 cycles at 300 mA·g^{-1} and a capacity retention of 95.7% (Figure 9(c)). The enhanced performance was ascribed to the optimized interlayer spacing and increased closed-pore density, underscoring the effectiveness of microstructural engineering in biomass-derived HC for SIBs.

Similarly, Xiao *et al.* [54] employed coconut shells as carbon precursors to synthesize HC (CSZ), incorporating $ZnCl_2$ to enlarge the interlayer spacing and create a closed-pore structure. This design strategy significantly enhanced Na^+ storage capacity. The resulting CSZ anode demonstrated excellent electrochemical performance, maintaining a reversible capacity of 310.0 mAh·g^{-1} with 88.1% retention after 50 cycles. This work underscores how biomass-derived HCs can be tailored with chemical activation agents to optimize sodium storage capability. Gao *et al.* [70] reported the use of orange peel as a carbon precursor via hydrothermal and subsequent high-temperature carbonization. Their study revealed that the interlayer spacing decreased as the carbonization temperature increased, reflecting a transition toward a more ordered microstructure. Among the tested samples, HC-1300 exhibited the most favorable electrochemical performance. Specifically, it delivered a reversible capacity of 234.0 mAh·g^{-1} at 500 mA·g^{-1} and retained 98.7% of its capacity over 500 cycles, demonstrating excellent long-term stability. This example highlights the critical role of carbonization temperature in balancing structural order and electrochemical performance.

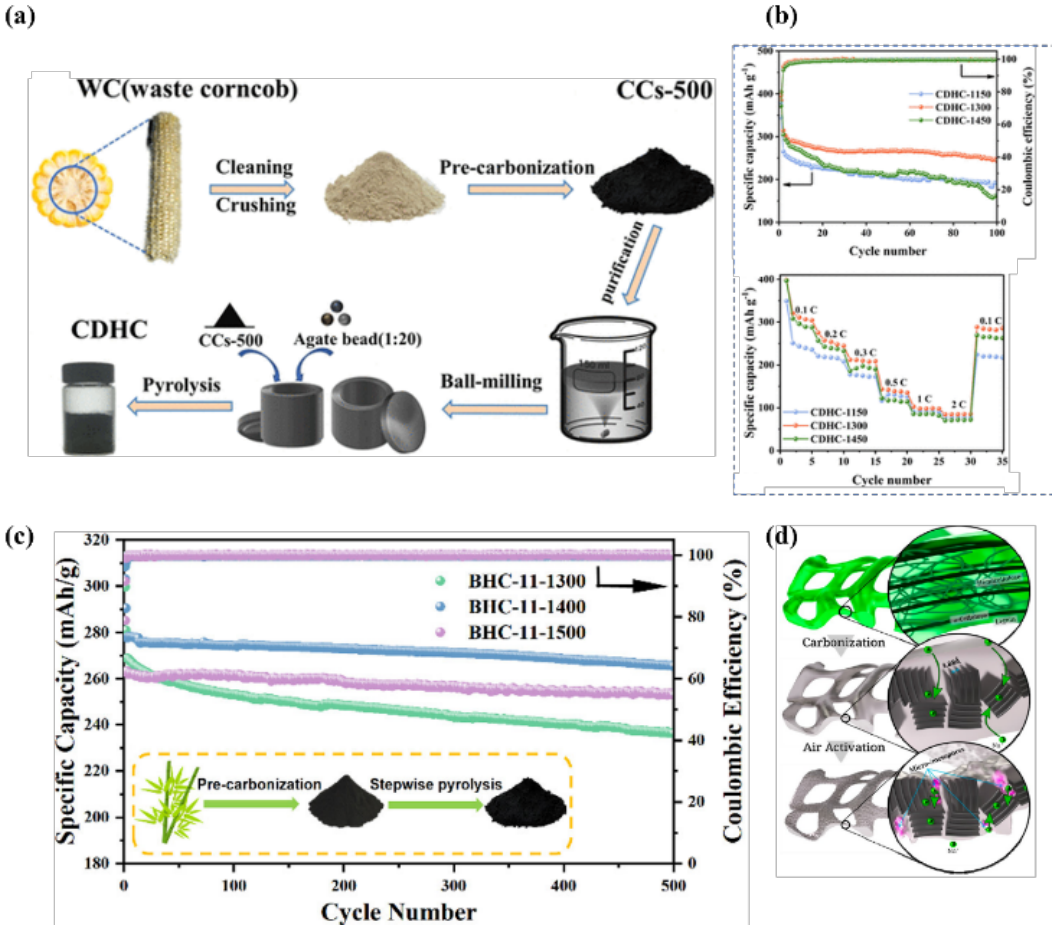

Figure 9. (a) The fabrication process of CCs, (b) The rate performance and the stability of CCs (Reproduced with permission from ref. [73]. Copyright 2024, ACS), (c) The stability performance of the BHC electrode (Reproduced with permission from ref. [74]. Copyright 2025, ACS), and (d) The structure of HC, which is made by peat moss (Reproduced with permission from ref. [75]. Copyright 2013, ACS).

In another study, Ding *et al.* [75] synthesized HC from peat moss, one of the most diverse plant species on Earth. Benefiting from its natural porous cellular structure rich in lignin and hemicellulose, the derived carbon exhibited a large open framework that facilitated Na^+ insertion and diffusion, thereby improving overall electrochemical performance (Figure 9(d)). Likewise. Guo *et al.* [1] investigated camphor wood sawdust as a precursor and systematically examined the influence of heating rate. Their results indicated that a slower heating rate (0.25°C·min^{-1}) suppressed excessive defect formation and minimized side reactions, leading to reduced SEI growth. The optimized HC electrode achieved an initial capacity of 324.6 mAh·g^{-1} at 0.05 A·g^{-1} and retained 90% capacity after 200 cycles, demonstrating superior stability. Waste maize cobs have also been successfully employed as precursors. Liu *et al.* [69] prepared HC via a simple pyrolytic carbonization route and reported reversible capacities of ~300 mAh·g^{-1} with an ICE of 86.0% at 0.1C. These findings suggest that inexpensive agricultural residues can be directly transformed into high-performance HC anodes with minimal processing.

Overall, agricultural and forestry by-products provide unique advantages due to their inherently porous and layered microstructures. During high-temperature treatment, crystalline cellulose decomposes into elongated and curved graphene-like layers, which evolve into closed-cell structures. Meanwhile, hemicellulose suppresses excessive graphitization, helping to retain structural disorder. As a result, the derived HC materials offer abundant defect sites and interlayer gaps for Na^+ storage and diffusion. Moreover, the chemical diversity of different precursors enables the tuning of pore structure, surface functionality, and electronic conductivity, which in turn tailors the electrochemical behavior.

Despite these merits, the performance of agricultural biomass-derived HCs is often challenged by the intrinsic heterogeneity of raw materials, seasonal variability, and batch-to-batch inconsistency. Future efforts may focus on combining agricultural residues with heteroatom doping, templating strategies, or hybridization with conductive phases to further enhance sodium storage performance. In addition, developing scalable pretreatment methods that improve feedstock uniformity while maintaining low cost will be critical to translating these laboratory successes into industrial-scale applications.

3.3 Marine life

With oceans covering more than 70% of the Earth's surface, marine ecosystems provide an abundant and renewable supply of biomass resources, including fish [76], shrimp, crabs [77], algae [2], and other marine organisms. Unlike terrestrial plants, marine biomass contains not only carbon, hydrogen, and oxygen but also substantial quantities of natural minerals and organic constituents such as nitrogen, phosphorus, calcium, and sulfur. Upon carbonization, these heteroatoms are often retained in the carbon matrix, leading to self-doped HC materials with enriched surface functionalities. Such intrinsic doping can effectively tune the electronic structure, increase the interlayer spacing, and generate abundant defect sites, thereby enhancing the electrochemical properties of HC for sodium-ion storage [77].

Heteroatom doping derived from marine biomass has been shown to influence both ionic and electronic transport [2]. For example, the introduction of fluorine, phosphorus, and sulfur atoms can enlarge the interlayer spacing of carbon and improve Na^+ diffusion kinetics [78]. Boron and nitrogen co-doping can introduce additional defect sites that enhance sodium adsorption capacity [3]. Similarly, oxygen, nitrogen, and phosphorus functionalities can contribute to improved electronic conductivity [79]. These synergistic effects enable marine biomass-derived HCs to exhibit superior charge storage capability compared to many land-based precursors [80].

A representative study by Zheng *et al.* [81] utilized chitosan extracted from crab shells as a precursor, followed by nitrogen doping with urea. The resulting carbon materials exhibited high surface area and significant nitrogen content while preserving the porous nanostructure of the chitosan framework (Figure 10(a-c)). Electrochemical testing revealed excellent performance: the electrode delivered specific capacities of 245.0 F·g^{-1} (three-electrode system) and 227.0 F·g^{-1} (two-electrode system) at 0.50 A·g^{-1}. Furthermore, the constructed supercapacitor retained 98.0% of its capacitance over 10,000 cycles (Figure 10(d)), demonstrating remarkable cycling stability and rate capability.

Similarly, Guo and others [76] directly carbonized squid bone, followed by air oxidation activation, to obtain a nitrogen/oxygen dual-doped porous HC structure (Figure 10(e-f)). The resulting electrode displayed outstanding long-term performance, maintaining 90.5% capacitance retention even after 8000 cycles at a high current density of 5000 mA·g^{-1} (Figure 10(g)). This enhanced cycling stability was attributed to the improved conductivity and increased ion transport pathways introduced by heteroatom doping and porous framework formation (Figure 10(h)).

Beyond crustacean-derived precursors, marine sponges and algae have also been explored. Meenatchi *et al.* [82] prepared HC from sponge biomass, which preserved the natural sponge-like porous morphology after carbonization (Figure 11(a)). The resulting materials showed excellent sodium storage behavior: at 0.1C, the K-SS, Na-SS, and Zn-SS electrodes achieved specific capacities of 321.4 mAh·g^{-1}, 334.9 mAh·g^{-1}, and 347.4 mAh·g^{-1}, respectively, reflecting their versatility for different ion storage systems. Meng *et al.* [83] investigated algal blooms as precursors, thereby transforming harmful waste biomass into valuable anode materials for SIBs. The derived carbon exhibited a spherical morphology resembling cyanobacterial cells (Figure 11(b)) and delivered a reversible capacity of 230.0 mAh·g^{-1} after 60 cycles at 0.02 A·g^{-1}, confirming both its practical performance and ecological benefits. Chen *et al.* [77] further reported that crab shell-derived HC possessed a honeycomb-like layered structure with abundant pores (Figure 11(c)). The formation of this framework was attributed to the decomposition of chitin nanofibers at elevated temperatures, which created a hierarchical pore system conducive to Na^+ transport.

Collectively, marine biomass-derived HCs benefit from their intrinsic heteroatom content, fibrous structures, and naturally porous morphologies, which result in high specific surface areas and multiple ion transport channels. Compared to conventional agricultural biomass (e.g., coconut shells), marine resources are often more sustainable, renewable, and potentially lower in cost. Importantly, utilizing invasive or waste marine organisms (e.g., algal blooms or discarded shells) can simultaneously address environmental issues while providing valuable functional materials.

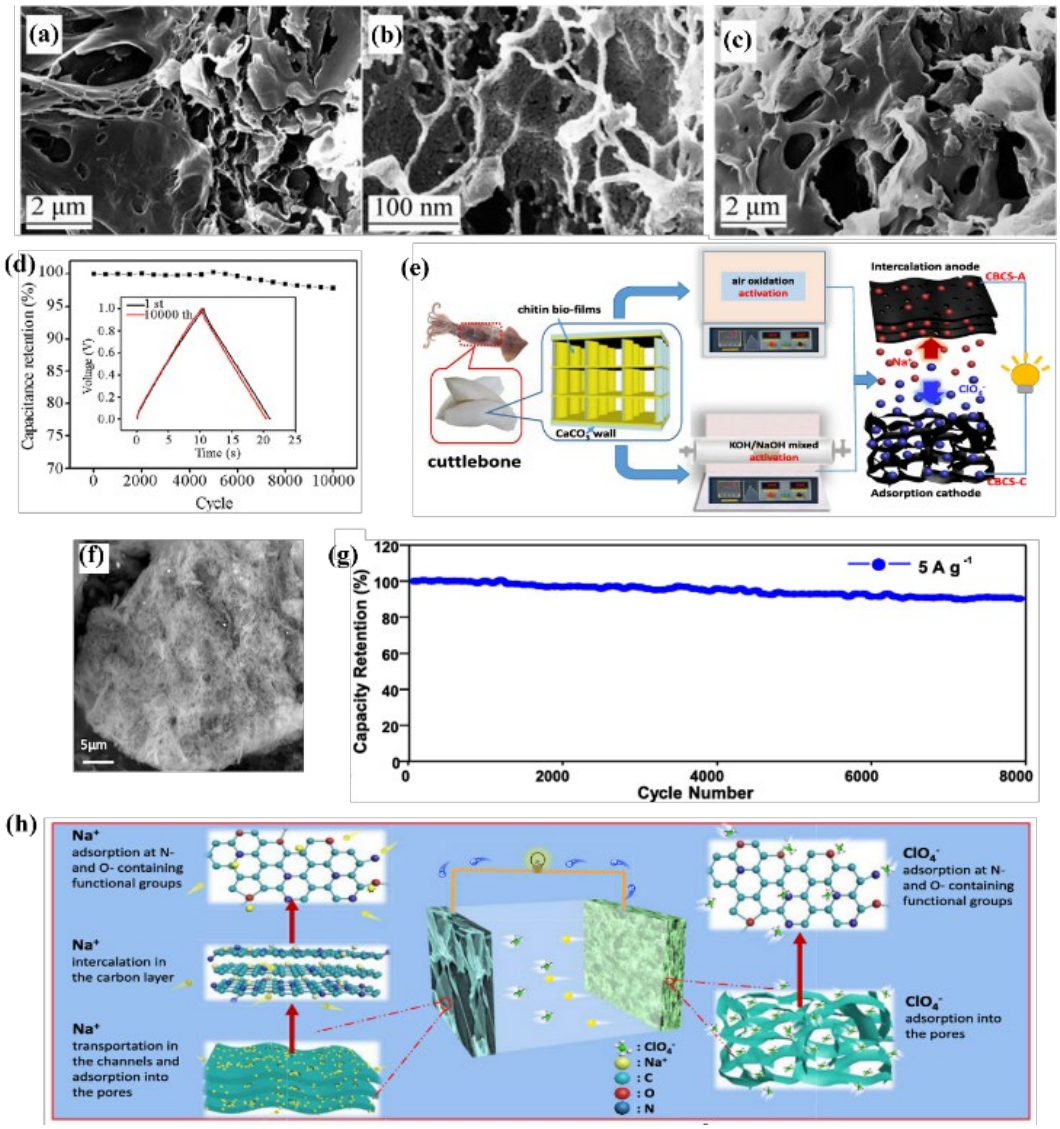

Figure 10. (a-c) The SEM images of HC, (d) The capacitance retention of HC (Reproduced from ref. [81]), (e) Fabrication process of HC, (f) The SEM images of HC, (g) The stability of HC electrode, (h) The mechanism of HC (Reproduced with permission from ref. [76]. Copyright 2018, ACS).

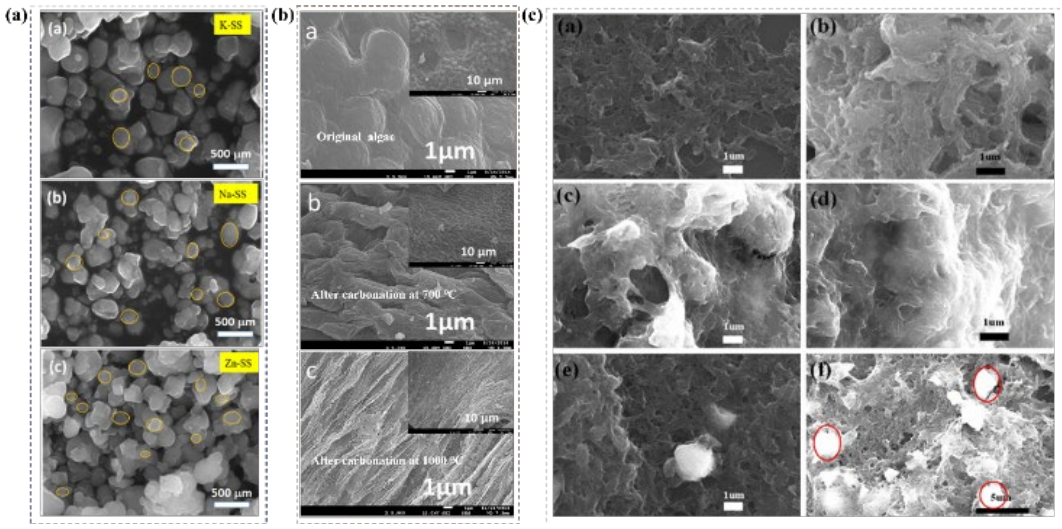

Figure 11. The SEM images of HC devised from (a) sponge (Reproduced from ref. [82]), (b) algal (Reproduced from ref. [83]), and (c) crab shells (Reproduced from ref. [77]).

Nevertheless, significant challenges remain for large-scale implementation. The regional accessibility of marine biomass is limited, with availability depending on coastal ecosystems. Furthermore, excessive heteroatom doping, while beneficial for conductivity and defect formation, may increase surface area and induce irreversible side reactions, ultimately reducing ICE [84]. Structural deformation during cycling due to heteroatom-induced stress also poses a risk for long-term stability.

Future research directions may include optimizing heteroatom doping levels to balance conductivity and ICE, designing hierarchical pore structures to mitigate volume changes, and combining marine-derived HCs with conductive additives or protective coatings to further enhance cycle stability. Life-cycle assessments and techno-economic analyses are also essential to evaluate the sustainability of scaling up marine biomass utilization for industrial sodium-ion battery applications

3.4 Industrial wastes

Common industrial waste precursors for HC synthesis include petroleum derivatives, coal tar [34], various discarded resins (such as phenolic and epoxy) [85], pulp, and cardboard from paper processing waste [86]. Compared with agricultural residues and marine biomass, HC derived from industrial waste generally exhibits higher carbon yield, more uniform composition, and superior specific capacity. Moreover, the conversion of such wastes into functional carbon electrodes contributes to both resource recycling and environmental sustainability. Typically, industrial-waste-derived HCs present a disordered layered-porous composite structure, which is favorable for Na^+ adsorption and intercalation.

For instance, Xu *et al.* [87] developed coal-derived HC via a low-temperature dry-ice-assisted ball milling strategy (Figure 12(a)), producing uniform nanoparticles with surface etching and abundant defects. As shown in Figure 12(b), the use of dry ice as the grinding medium resulted in a defect-rich surface and an enlarged interlayer spacing of 0.375 nm. The material exhibited a first reversible capacity of 308.1 $mAh \cdot g^{-1}$ at 30 $mA \cdot g^{-1}$ and retained 78% of its capacity after 500 cycles at 300 $mA \cdot g^{-1}$, with excellent rate performance (Figure 12(c)). Kinetic analysis indicated that the enhanced slope capacity and rate performance were closely related to the high defect density, demonstrating the effectiveness of defect engineering in improving the sodium storage properties of coal-based HCs.

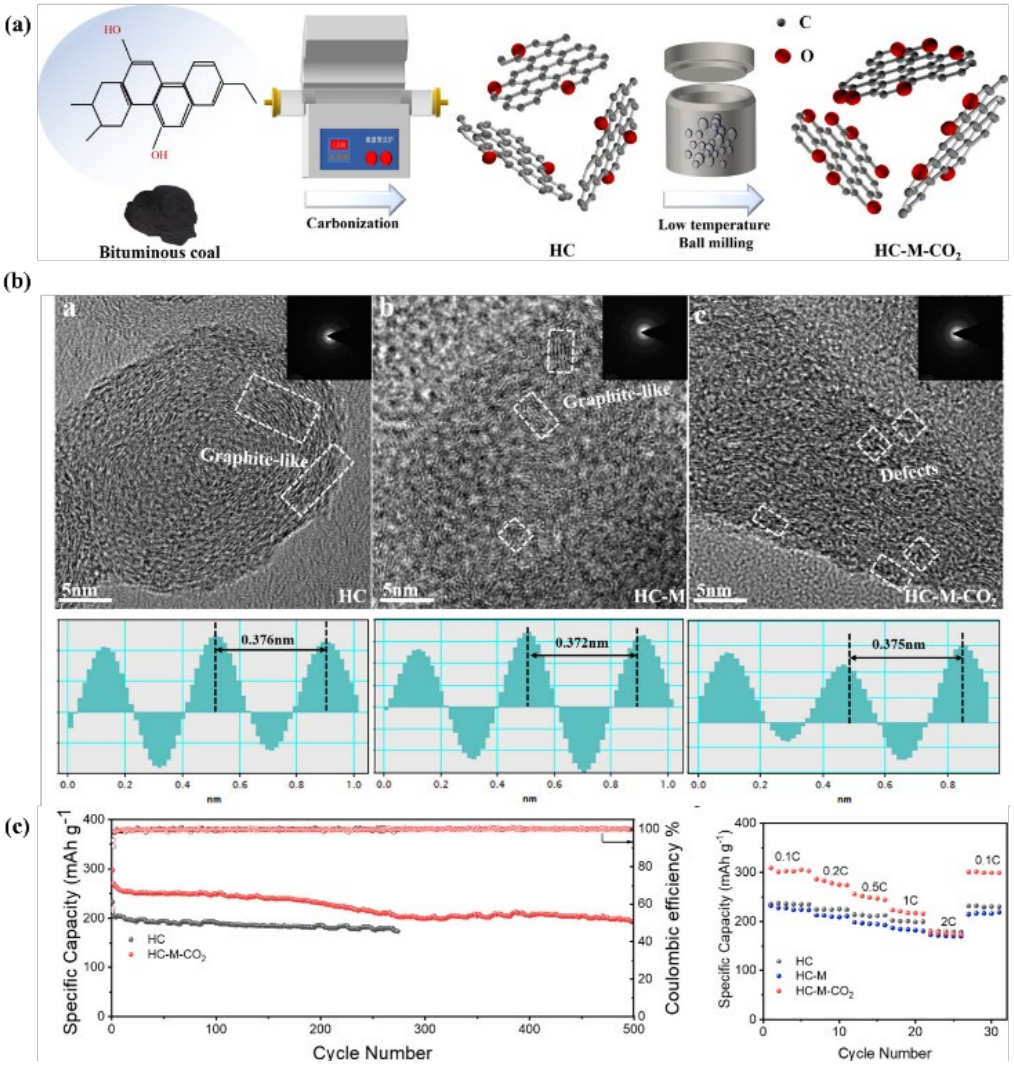

Figure 12. (a) the synthesis process of HC-M-CO_2, (b) HRTEM images of HC, HC-M, and HC-M-CO_2, (c) Cycling performance and rate performance of HC (Reproduced with permission from ref. [87]. Copyright 2025, ACS).

Similarly, Lv and co-workers [34] employed petroleum as a precursor to synthesize amorphous carbon for sodium-ion batteries. The resulting electrodes delivered excellent cycling stability and rate performance, achieving a reversible capacity of 270.0 mAh·g^{-1} with a maintained capacity of 252.0 mAh·g^{-1} at 100 mA·g^{-1} after 100 cycles. Interestingly, the proportion of the plateau region gradually increased with rising pyrolysis temperature, while the overall specific capacity decreased. This phenomenon can be attributed to reduced surface defects and decreased interlayer spacing at higher temperatures, which diminish Na^+ storage sites but improve structural stability. Li *et al.* [48] prepared HC anodes using anthracite (PA) through a simple pyrolysis and carbonization route. The PA-1200 electrode demonstrated outstanding electrochemical performance, achieving a reversible capacity of 222.0 mAh·g^{-1} at 0.2C with 89.0% retention after 600 cycles. Furthermore, a pouch cell fabricated with the PA anode achieved an actual energy density of 100.0 Wh·kg^{-1} and stable cycling behavior, highlighting its potential for practical large-scale applications.

Resin-based wastes have also been extensively investigated. Phenolic resin, in particular, is a widely available industrial product with high carbon yield, tunable structural design, and good thermal stability, making it a promising precursor for SIB anodes [88]. Liu *et al.* [85] synthesized HC materials from phenolic resin and optimized electrode performance by controlling the thickness of a soft carbon coating layer via asphalt addition. The resulting electrodes delivered an ICE of 88.20% and a reversible capacity of 309.80 mAh·g^{-1} at 0.015 A·g^{-1}, demonstrating both high initial efficiency and excellent long-term cycling stability. In another study, Kamiyama *et al.* [89] examined phenolic resin-derived HC prepared under different pyrolysis temperatures. Their results revealed that the specific surface area decreased with higher treatment temperatures, as open pores gradually transformed into closed-pore structures. Under optimized conditions, the electrode achieved an impressive initial capacity of 386.0 mAh·g^{-1} with an ICE of 85.0% at 0.01 A·g^{-1}, illustrating the strong potential of resin-based waste for HC fabrication.

Overall, HCs derived from industrial waste precursors exhibit high carbonization efficiency, competitive specific capacities, and stable structural frameworks, making them attractive candidates for scalable anode production. However, several challenges remain. Compared with agricultural or marine biomass, industrial waste processing is often more costly, as additional purification steps are required. For example, asphalt-based precursors typically demand cross-linking agents, while resin-based materials can release toxic volatile compounds (e.g., phenol) during pyrolysis, necessitating specialized exhaust treatment. These extra steps increase process complexity, preparation time, and overall costs. Therefore, future research should aim to optimize green synthesis strategies, minimize harmful byproducts, and improve ICE through defect engineering and controlled pore structure design. By addressing these challenges, industrial-waste-derived HC can serve as a reliable and sustainable precursor for sodium-ion batteries.

3.5 Summary

Overall, biomass materials derived from agricultural and forestry by-products remain the primary candidates for HC anode materials. These sources are inexpensive, widely available, and relatively easy to process, while providing high specific capacity and large surface area, making them suitable for industrialization. However, they also face challenges such as seasonal variation, unstable supply, low ICE, and batch-to-batch inconsistency. Marine biomass, as an emerging precursor, offers unique structural and chemical advantages, including a natural abundance of heteroatoms (e.g., N, O, P, S) and porous architectures that enhance Na^+ diffusion and conductivity. Nevertheless, their large-scale application is limited by geographical distribution, the need for pretreatment, and potential drawbacks such as reduced ICE or material deformation caused by heteroatom doping. Industrial waste-derived precursors, such as petroleum, coal tar, and resins, provide high carbon yield, stable raw material supply, and tunable structures, making them well-suited for controlled HC preparation. Yet, the higher costs, complex processing steps, and environmental concerns related to emissions and wastewater remain significant barriers for sustainable large-scale production (Figure 13).

A comparative summary of the three types of biomass-derived precursors is presented in Table 2, which highlights their distinctive features, advantages and limitations.

In conclusion, biomass precursors from agricultural and forestry by-products, marine biomass, and industrial wastes each present distinctive advantages and challenges for HC synthesis. Agricultural biomass offers the most promising large-scale pathway due to cost and abundance, marine biomass provides unique heteroatom-doping effects, and industrial wastes enable stable and controlled HC production but raise environmental and cost concerns.

Table 2. Comparison of biomass-derived precursors for HC synthesis.

Precursor type	Typical sources	Structural features	Advantages	Challenges
Agricultural and forestry by-products	Straw, rice husks, corn cobs, wood chips, fruit shells	Rich in cellulose/hemicellulose/ lignin; porous and layered; disordered carbon layers after pyrolysis	Abundant, low-cost, geographically widespread; simple preparation; good capacity and surface area	Seasonal supply fluctuations; precursor heterogeneity; low ICE; batch-to-batch variability
Marine biomass	Fish, shrimp/crab shells, algae, sponges	Naturally doped with heteroatoms (N, O, P, S); fibrous porous structure	Abundant in functional groups; heteroatom doping enhances conductivity and ion diffusion; renewable and low-cost	Geographical constraints; pretreatment required; high surface area may lower ICE; structural deformation upon cycling
Industrial wastes	Petroleum, coal tar, phenolic/epoxy resins, pulp waste	Disordered layered–porous composites; high carbon yield	High initial capacity; controllable structure; stable supply; suitable for industrialization	Higher cost; complex processing (e.g., gas treatment); potential environmental concerns (wastewater/emissions)

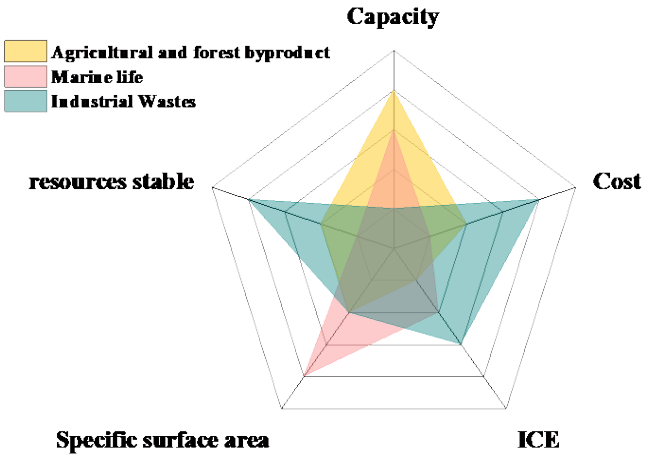

Figure 13. A comparison of biomass-derived precursors.

4. Perspectives and conclusions

4.1 Conclusions

In this review, we have systematically summarized recent advances in HC as anode materials for SIBs. We first introduced the fundamental advantages of SIBs over lithium-ion systems, including lower cost, resource abundance, and comparable theoretical capacity, followed by a discussion of the critical role of anode materials. Particular attention was devoted to HC, which remains the most promising anode candidate for commercial SIBs due to its tunable structure, abundant precursor sources, and relatively high electrochemical performance. We highlighted the structural characteristics of HC and analyzed different sodium storage models, including the intercalation–adsorption, adsorption–intercalation, pore-filling, and combined models, to clarify the complexity of Na^+ storage mechanisms in carbonaceous materials.

A key focus of this review was the precursor-dependent synthesis of HC. Different biomass-derived precursors lead to significant variations in carbon microstructure, porosity, and heteroatom doping, thereby strongly affecting electrochemical properties. Agricultural and forestry by-products represent the most abundant and economically viable sources, offering low-cost and scalable production. Marine biomass introduces unique nitrogen-, oxygen-, and phosphorus-rich structures that can enhance sodium storage kinetics, though geographical constraints and pretreatment requirements limit large-scale application. Industrial wastes, such as petroleum, coal tar, and phenolic resins, provide relatively stable carbon yields and high initial specific capacities, but the associated processing costs and environmental concerns (e.g., volatile emissions, wastewater) remain non-negligible. Overall, the choice of precursor not only governs the physicochemical properties of HC but also determines its feasibility for practical deployment.

4.2 Opportunities and challenges

Despite substantial progress, the industrialization of HC still faces several challenges:

1) Structural uniformity and reproducibility: The electrochemical performance of HC is highly sensitive to precursor composition and processing conditions. Agricultural and forestry precursors are affected by seasonal and regional variations, resulting in batch-to-batch inconsistencies. Controlling carbonization temperature, heating rate, and activation parameters is essential to ensure reproducible material properties.

2) Initial Coulombic efficiency and energy loss: Many biomass-derived HCs exhibit relatively low ICE due to excessive surface area, defects, and unstable SEI formation. This issue remains a bottleneck for large-scale application, especially in full-cell configurations where irreversible sodium consumption severely reduces energy density.

3) Scalability and cost: Although biomass resources are abundant, the processing requirements (e.g., purification, heteroatom doping, structural modification) often increase production costs. Industrial wastes offer a stable supply but may involve energy-intensive treatments and environmental management (e.g., exhaust gas purification).

4) Environmental and sustainability considerations: The sustainability of HC production depends not only on precursor selection but also on the carbonization and activation processes which may generate secondary pollution. Developing green, low-energy processes is crucial to balance performance with environmental responsibility.

Overall, biomass-derived HC represents a versatile and sustainable pathway for the development of next-generation SIB anodes. Each precursor type offers unique advantages and faces distinct challenges. A holistic approach integrating precursor selection, structural engineering, scalable synthesis, and environmental considerations will be essential for advancing HC toward commercial application. With continuous innovations in materials science, process optimization, and device integration, HC is expected to play a pivotal role in enabling cost-effective, sustainable, and high-performance sodium-ion batteries in the near future.

Acknowledgements

This work was supported by Thailand Science Research and Innovation Fund Chulalongkorn University (INDFF691442300035). Anqi Lu would like to acknowledge the support from China Scholarship Council, China.

References

[1] S. Guo, Y. Chen, L. Tong, Y. Cao, H. Jiao, Z. Iong, X. and Qiu, "Biomass hard carbon of high initial coulombic efficiency for sodium-ion batteries: Preparation and application," *Electrochimica Acta*, vol. 410, p. 140017, 2022.

[2] E. Gibertini, F. Liberale, C. Dossi, G. Binda, B. Mattioli, R. Rettinetti, A. Maspero, M. Fiore, R. Ruffo, and L. Magagnin, "Algae-derived hard carbon anodes for Na-ion batteries," *Journal of Applied Electrochemistry*, vol. 51, no. 12, pp. 1665–1673, 2021.

[3] M. Thompson, Q. Xia, Z. Hu, and X. S. Zhao, "A review on biomass-derived hard carbon materials for sodium-ion batteries," *Materials Advances*, vol. 2, no. 18, pp. 5881–5905, 2021.

[4] C. Nita, B. Zhang, J. Dentzer, and C. M. Ghimbeu, "Hard carbon derived from coconut shells, walnut shells, and corn silk biomass waste exhibiting high capacity for Na-ion batteries," *Journal of Energy Chemistry*, vol. 58, pp. 207–218, 2021.

[5] A. Vasileiadis, Y. Li, Y. Lu, Y. S. Hu, and M. Wagemaker, "Role of defects, pores, and interfaces in deciphering the alkali metal storage mechanism in hard carbon," *ACS Applied Energy Materials*, vol. 6, no. 1, pp. 127–140, 2023.

[6] T. Yin, Z. Zhang, L. Xu, C. Li, and D. Han, "Preparation of green high-performance biomass-derived hard carbon materials from bamboo powder waste," *ChemistryOpen*, vol. 13, no. 5, p. e202300178, 2024.

[7] B. Zhong, C. Liu, D. Xiong, J. Cai, J. Li, D. Li, Z. Cao, B. Song, W. Deng, H. Peng, H. Hou, G. Zou, and X. Ji, "Biomass-derived hard carbon for sodium-ion batteries: Basic research and industrial application," *ACS Nano*, vol. 18, no. 26, pp. 16468–16488, 2024.

[8] M. Yuan, B. Cao, H. Liu, C. Meng, J. Wu, S. Zhang, A. Li, X. Chen, and H-H. Song, "Sodium Storage mechanism of non-graphitic carbons: A general model and the function of accessible closed pores," *Chemistry of Materials*, vol. 34, no. 7, pp. 3489–3500, 2022.

[9] Y. Liu, "Techno-economic analysis of biomass conversion to hard carbon materials," *Master thesis*, 2022.

[10] S. Tan, H. Yang, Z. Zhang, X. Xu, Y. Xu, J. Zhou, X. Zhou, Z. Pan, X. Rao, Z. Wang, Y. Wu, X. Liu, and Y. Zhang, "The progress of hard carbon as an anode material in sodium-ion batteries," *Molecules*, vol. 28, no. 7, p. 3134, 2023.

[11] N. Nieto, J. Porte, D. Saurel, L. Djuandhi, N. Sharma, A. Lopez-Urionabarrenechea, V. Palomares, and T. Rojo, "Use of hydrothermal carbonization to improve the performance of biowaste-derived hard carbons in sodium ion-batterie," *ChemSusChem*, vol. 16, no. 23, p. e202301053, 2023.

[12] A. Rehman, S. Saleem, S. Ali, S. M. Abbas, M. Choi, and W. Choi, "Recent advances in alloying anode materials for sodium-ion batteries: Material design and prospects," *Energy Materials*, vol. 4, no. 6, p. 400068, 2024.

[13 M. Bhar, S. Ghosh, and S. K. Martha, "Designing freestanding electrodes with Fe_2O_3-based conversion type anode material for sodium-ion batteries," *Journal of Alloys and Compounds*, vol. 948, no. 5, p. 169670, 2023.

[14] S. You, Q. Zhang, J. Liu, Q. Deng, Z. Sun, D. Cao, L. Tongchao, K. Amine, and C. Yang, "Hard carbon with an opened pore structure for enhanced sodium storage performance," *Energy & Environmental Science*, vol. 17, no. 21, pp. 8189–8197, 2024.

[15] X. Wang, X. Zhao, and L. Wang, "Bulk alloy anodes for sodium-ion batteries," *Batteries & Supercaps*, vol. 8, no. 4, p. e202400551, 2024.

[16] M. Lao, Y. Zhang, W. Luo, Q. Yan, W. Sun, and S. X. Dou, "Alloy-based anode materials toward advanced sodium-ion batteries," *Advanced Materials*, vol. 29, no. 48, pp. 1–23, 2017.

[17] S. A. Riza, R. G. Xu, Q. Liu, M. Hassan, Q. Yang, D. B. Mu, L. Li, F. Wu, and R. J. Chen, "A review of anode materials for sodium ion batteries," *New Carbon Materials*, vol. 39, no. 5, pp. 743–769, 2024.

[18] H. Xu, H. Li, and X. Wang, "The anode materials for lithium-ion and sodium-ion batteries based on conversion reactions: A review," *ChemElectroChem*, vol. 10, no. 9, p. e202201151, 2023.

[19] A. Skurtveit, A. Brennhagen, H. Park, C. Cavallo, and A. Y. Koposov, "Benefits and development challenges for conversion-alloying anode materials in na-ion batteries," *Frontiers in Energy Research*, vol. 10, pp. 1–7, 2022.

[20] L. Fang, N. Bahlawane, W. Sun, H. Pan, B. Xu, M. Yan, and Y. Jiang, "Conversion-alloying anode materials for sodium ion batteries," *Small*, vol. 17, no. 37, pp. 1–38, 2021.

[21] H-Y. Hu, Y. Xiao, W. Ling, Y-B. Wu, P. Wang, T. Shuang-Jie, Y-S. Xu, Y-J. Guo, W-P. Chen, R-R. Tang, X-X. Zeng, Y-X. Yin, and X-W. Wu, "A stable biomass-derived hard carbon anode for high-performance sodium-ion full battery," *Energy Technology*, vol. 9, no. 1, pp. 1–7, 2021.

[22] M. Kitta, R. Kataoka, S. Tanaka, N. Takeichi, and M. Kohyama, "Spinel-type sodium titanium oxide: A promising sodium-insertion material of sodium-ion batteries," *ACS Applied Energy Materials*, vol. 2, no. 6, pp. 4345–4353, 2019.

[23] X. Chen, C. Liu, Y. Fang, X. Ai. F. Zhong, H. Yang, and Y. Cao, "Understanding of the sodium storage mechanism in hard carbon anodes," *Carbon Energy*, vol. 4, no. 3, pp. 1133–1150, 2022.

[24] S. Park, J. Song, W. C. Lee, S. H. Jang, J. Lee, J. Kim, H-K. Kim, and K. Min, "Advances in biomass-derived electrode materials for energy storage and circular carbon economy," *Chemical Engineering Journal*, vol. 470, no. 4, p. 144234, 2023.

[25] G. Li, H. Ma, Y. Tong, H. Wang, Y. Luo, E. H. Ang, S. Bohm, A. A. Ibrahim, and A. Umar, "Research progress on carbon-based anode materials for sodium-ion batteries," *Journal of Energy Storage*, vol. 107, p. 114977, 2025.

[26] X. Tan, K. Jiang, S. Zhai, J. Zhou, J. Wang, K. Cadien, and Z. Li, "X-ray spectromicroscopy investigation of heterogeneous sodiation in hard carbon nanosheets with vertically oriented (002) planes," *Small*, vol. 17, no. 52, pp. 1–11, 2021.

[27] L. K. Iglesias, E. N. Antonio, T. D. Marinez, L. Zhang, Z. Zhuo, S. J. Weigand, J. Guo, and M. F. Toney, "Revealing the sodium storage mechanisms in hard carbon pores," *Advanced Energy Materials*, vol. 13, no. 44, pp. 1–13, 2023.

[28] L. Zhou, Y. Cui, P. Niu, L. Ge, R. Zheng, S. Liang, and W. Xing, "Biomass-derived hard carbon material for high-capacity sodium-ion battery anode through structure regulation," *Carbon N. Y.*, vol. 231, p. 119733, 2025.

[29] L. Dai, D. W. Chang, J. B. Baek, and W. Lu, "Carbon nanomaterials for advanced energy conversion and storage," *Small*, vol. 8, no. 8, pp. 1130–1166, 2012.

[30] A. Bachmatiuk, J. J. Boeckl, H. Smith, I. Ibrahim, T. Gemming, S. Oswald, W. Kazmierczak, D. Makarov, O. G. Schmidt, J. Eckert, L. Fu, and M. H. Rümmeli, "Vertical graphene growth from amorphous carbon films using oxidizing gases," *The Journal of Physical Chemistry C*, vol. 119, no. 31, pp. 17965–17970, 2015.

[31] L. Lower, S. C. Dey, T. Vook, M. Nimlos, S. Park, and W. J. Sagues, "Catalytic graphitization of biocarbon for lithium-ion anodes: A minireview," *ChemSusChem*, vol. 16, no. 24, p. e202300729, 2023.

[32] H. Liu, J. Chen, S. Qiao, and W. Zhang, "Carbon-based nanomaterials for bone and cartilage regeneration: A review," *ACS Biomaterials Science & Engineering*, vol. 7, no. 10, pp. 4718–4735, 2021.

[33] J. H. Lv, J-S. Wang, B. He, W. Tao, A-H. Lu, W. Zhang, J. Xu, W. Yin, G-P. Hao, and W-C. Li, "Revealing an extended

adsorption/insertion-filling sodium storage mechanism in petroleum coke-derived amorphous carbon," *Advanced Science*, vol. 11, no. 42, p. 2407538, 2024.

[34] H. Tian, M. Graczyk-Zajac, A. Kessler, A. Weidenkaff, and R. Riedel, "Recycling and reusing of graphite from retired lithium-ion batteries: A Review," *Advanced Materials*, vol. 36, no. 13, pp. 1–30, 2024.

[35] M. Chen, Z. Wang, Y. Wang, Y. Li, and Q. Chen, "Sodium-ion storage mechanisms and design strategies of molybdenum-based materials: A review," *Applied Materials Today*, vol. 23, p. 100985, 2021.

[36] E. Kim, R. K. Petla, Z. T. Gossage, K. Kubota, T. Hosaka, R. Tatara, and S. Komaba, "Active material and interphase structures governing performance in sodium and potassium ion batteries," *Chemical Science*, vol. 13, no. 21, pp. 6121–6158, 2022.

[37] D. Kang, H. K. Kim, H. J. Kim, and Y. Han, "Preparation of biomass-derived hard carbon with uniform ultramicropores for development of fast charging Li-ion batteries," *Journal of Alloys and Compounds*, vol. 900, p. 163420, 2022.

[38] Y. Aniskevich, J. H. Yu, J. Y. Kim, S. Komaba, and S. T. Myung, "Tracking sodium cluster dynamics in hard carbon with a low specific surface area for sodium-ion batteries," *Advanced Energy Materials*, vol. 14, no. 18, p. 2304300, 2024.

[39] N. Sun, J. Qiu, and B. Xu, "Understanding of sodium storage mechanism in hard carbons: Ongoing Development under debate," *Advanced Energy Materials*, vol. 12, no. 27, pp. 1–39, 2022.

[40] Y. Ge, Y. Qiu, J. Han, S. Mirza, H. Liu, G. Zhong, Q. Zheng, Z. Peng, and X. Li, "Insights into the dynamical sodium occupancy evolution and rate-limiting steps in hard carbon," *Journal of the American Chemical Society*, vol. 147, no. 43, pp. 39537–39546, 2025.

[41] D. A. Stevens, and J. R. Dahn, "The Mechanisms of lithium and sodium insertion in carbon materials," *Journal of The Electrochemical Society*, vol. 148, no. 8, p. A803, 2001.

[42] S. Komaba, W. Murata, T. Ishikawa, N. Yabuuchi, T. Ozeki, T. Nakayama, A. Ogata, K. Gotoh, and K. Fujiwara, "Electrochemical Na insertion and solid electrolyte interphase for hard-carbon electrodes and application to Na-ion batteries," *Advanced Functional Materials*, vol. 21, no. 20, pp. 3859–3867, 2011.

[43] Y. Morikawa, S. ichi Nishimura, R. ichi Hashimoto, M. Ohnuma, and A. Yamada, "Mechanism of sodium storage in hard carbon: An x-ray scattering analysis," *Advanced Energy Materials*, vol. 10, no. 3, pp. 1–9, 2020.

[44] Y. Cao, L. Xiao, M. L. Sushko, W. Wang, B. Schwenzer, J. A. Xiao, Z. Nie, L. Saraf, Z. Yang, and J. Liu, "Sodium ion insertion in hollow carbon nanowires for battery applications," *Nano Letters*, vol. 12, no. 7, pp. 3783–3787, 2012.

[45] Y. Luo, Y. Xu, X. Li, K. Zhang, Q. Pang, and A. Qin, "Boosting the Initial coulomb efficiency of sisal fiber-derived carbon anode for sodium ion batteries by microstructure controlling," *Nanomaterials*, vol. 13, no. 5, p. 881, 2023.

[46] X. Chen, Y. Fang, H. Lu, L. Hui, X. Feng, W. Chen, X. Ai. H. Yang, and Y. Cao, "Microstructure-dependent charge/discharge behaviors of hollow carbon spheres and its implication for sodium storage mechanism on hard carbon anodes," *Small*, vol. 17, no. 34, pp. 1–9, 2021.

[47] Y. Li, Y-S. Hu, X. Qi, X. Rong, H. Li, X. Huang, and L. Chen, "Advanced sodium-ion batteries using superior low cost pyrolyzed anthracite anode: towards practical applications," *Energy Storage Materials*, vol. 5, pp. 191–197, 2016.

[48] P. Bai, Y. He, X. Zou, X. Zhao, P. Xiong, and Y. Xu, "Elucidation of the sodium-storage mechanism in hard carbons," *Advanced Energy Materials,*, vol. 8, no. 15, pp. 1–9, 2018.

[49] C. Bommier, T. W. Surta, M. Dolgos, and X. Ji, "New mechanistic insights on na-ion storage in nongraphitizable carbon," *Nano Letters*, vol. 15, no. 9, pp. 5888–5892, 2015.

[50] J. Li, C. Peng, J. Li, J. Wang, and H. Zhang, "Insight into sodium storage behaviors in hard carbon by ReaxFF molecular dynamics simulation," *Energy and Fuels*, vol. 36, no. 11, pp. 5937–5952, 2022.

[51] E. M. Reynolds, J. Fitzpatrick, M. O. Jones, N. Tapia-Ruiz, H. Y. Playford, S. Hull, I. McClelland, P. J. Baker, S. A. Cussen, and G. E. Pérez, "Investigation of sodium insertion in hard carbon with operando small angle neutron scattering," *Journal of Materials Chemistry A*, vol. 12, no. 12, pp. 18469–18475, 2024.

[52] Y. Chen, G. Peng, M. Zhao, Y. Zhou, Y. Zeng, H. B. He, and J. Zeng, "Dual-element synergy driven breakthrough in sodium storage performance of phenolic resin-based hard carbon," *Carbon N. Y.*, vol. 238, p. 120269, 2025.

[53] H. Xiao, F. Wang, J. Peng, J. Luo, H. Li, Z. Wang, X. Luo, and Y. Chen, "Zinc-assisted modification of hard carbon for enhanced sodium-ion storage," *Journal of Electroanalytical Chemistry*, vol. 978, p. 118889, 2025.

[54] Y. Li, A. Vasileiadis, Q. Zhou, Y. Lu, Q. Meng, Y. Li, P. Ombrini, J. Zhao, X. Chen, Y. Niu, X. Qi, F. Xie, R. v. d. Jagt, S. Ganapathy, M-M. Titirci, H. Li, L. Chen, M. Wagemaker, and Y-S. Hu, "Origin of fast charging in hard carbon anodes," *Nature Energy*, vol. 9, no. 2, pp. 134–142, 2024.

[55] B. Pei, H. Yu, L. Zhang, F. Guozhao, J. Zhou, C. Xinxin, and S. Liang, "Hard carbon for sodium-ion batteries: From fundamental research to practical applications," *Advanced Materials*, vol. 37, no. 39, p. 2504574, 2025.

[56] Z. Zhu, and Z. Xu, "The rational design of biomass-derived carbon materials towards next-generation energy storage: A review," *Renewable and Sustainable Energy Reviews*, vol. 134, p. 110308, 2020.

[57] T. A. Khan, A. S. Saud, S. S. Jamari, M. H. A. Rahim, J. W. Park, and H. J. Kim, "Hydrothermal carbonization of lignocellulosic biomass for carbon rich material preparation: A review," *Biomass and Bioenergy*, vol. 130, p. 105384, 2019.

[58] J. Yin, Y. S. Zhang, H. Liang, W. Zhang, and Y. Zhu, "Synthesis strategies of hard carbon anodes for sodium-ion batteries," *Materials Reports: Energy*, vol. 4, no. 2, p. 100268, 2024.

[59] J. Huo, C. Li, P. Xia, N. Fan, W. Mao, and K. Bao, "Preparation of hard carbon from acid-treated locust wood as anode material for sodium-ion batteries," *Journal of Applied Electrochemistry*, vol. 55, no. 5, pp. 1099–1110, 2024.

[60] Z. Hou, D. Lei, M. Jiang, Y. Gao, X. Zhang, Y. Zhang, and J-G. Wang, "Biomass-derived hard carbon with interlayer spacing

optimization toward ultrastable Na-ion storage," *ACS Applied Materials & Interfaces*, vol. 15, no. 1, pp. 1367–1375, 2023.

[61] B. Yan, C. Han, Y. Dai, M. Li, Z. Wu, and X. Gao, "Biomass derived hard carbon materials for sodium ion battery anodes: Exploring the influence of carbon source on structure and sodium storage performance," *Fuel*, vol. 371, p. 132141, 2024.

[62] T. A. Khan, A. S. Saud, S. S. Jamari, M. H. A. Rahim, J. W. Park, and H. J. Kim, "Hydrothermal carbonization of lignocellulosic biomass for carbon rich material preparation: A review," *Biomass and Bioenergy*, vol. 130, p. 105384, 2019.

[63] Z. Zhu, Y. Men, W. Zhang, W. Yang, F. Wang, Y. Zhang, Y Zhang, X. Zeng, J. Xiao, T. Cheng, X. Li, and Y. Zhang, "Versatile carbon-based materials from biomass for advanced electrochemical energy storage systems," *eScience*, vol. 4, no. 5, p. 100249, 2024.

[64] N. Wang, Y-Y. Liu, Z-X. Shi, Z-L. Yu, H-Y. Duan, S. Fang, J-Y. Yang, and X-M. Wang, "Electrolytic silicon/graphite composite from SiO_2/graphite porous electrode in molten salts as a negative electrode material for lithium-ion batteries," *Rare Metals,* vol. 41, no. 9, pp. 438–447, 2022.

[65] M. Cavali, N. L. Junior, J. D. de. Sena, A. L. Woiciechowski, C. R. Soccol, P. B. Filho, R. Bayard, H. Benbelkacem, S. B. de. C. Junior, "A review on hydrothermal carbonization of potential biomass wastes, characterization and environmental applications of hydrochar, and biorefinery perspectives of the process," *Science of The Total Environment*, vol. 857, p. 159627, 2023.

[66] D. Burova, I. Shakhova, P. Morozova, A. Iarchuk, O. A. Drozhzhin, M. G. Rozova, S. Praneetha, V. Murugan, J-M. Tarascon, and A. M. Abakumov, "The rapid microwave-assisted hydrothermal synthesis of NASICON-structured $Na_3V_2O_{2x}(PO_4)_2F_{3-2x}$ $(0 < x \leq 1)$ cathode materials for Na-ion batteries," *RSC Advances*, vol. 9, no. 34, pp. 19429–19440, 2019.

[67] P. Liu, Y. Li, Y. S. Hu, H. Li, L. Chen, and X. Huang, "A waste biomass derived hard carbon as a high-performance anode material for sodium-ion batteries," *Journal of Materials Chemistry A*, vol. 4, no. 34, pp. 13046–13052, 2016.

[68] Y. Gao, S. Piao, C. Jiang, and Z. Zou, "Navel orange peel-derived hard carbons as high performance anode materials of Na and Li-ion batteries," *Diamond and Related Materials*, vol. 129, p. 109329, 2022.

[69] B. Valorization, F. Production, A. Lazzarini, R. Colaiezzi, F. Gabriele, and M. Crucianelli, "Support – Activity relationship in heterogeneous catalysis for biomss valorization and fine-chemicals production," *Materials (Basel).*, vol. 14, no. 22, p. 6796, 2021.

[70] S. Liu, A. Wang, Y. Liu, W. Zhou, H. Wen, H. Zhang, K. Sun, S. Li, J. Zhou, Y. Wang, J. Jiang, and B. Ii, "Catalytically active carbon for oxygen reduction reaction in energy conversion: Recent advances and future perspectives," *Advanced Science*, vol. 11, no. 22, pp. 1–64, 2024.

[71] Y. Tang, J. He, J. Peng, J. Yang, Z. Wu, P. Liu, K. Zhou, S. Hu, L. Hu, and X. Wang, "Electrochemical behavior of the biomass hard carbon derived from waste corncob as a sodium-ion battery anode," *Energy & Fuels*, vol. 38, no. 8, pp. 7389–7398, 2024.

[72] K. Zhou, J. Peng, Y. Tang, J. Yang, L. He, P. Liu, W. Qiu, L. Hu, L. Zheng, Q. Wei, and X. Wang, "Dual-tuned bamboo-derived hard carbon via stepwise pyrolysis for high-efficiency sodium-ion storage," *ACS Sustainable Chemistry & Engineering*, vol. 13, no. 34, pp. 13772–13782, 2025.

[73] J. Ding, H. Wang, Z. Li, A. Kohandehghan, K. Cui, Z. Xu, B. Zahiri, X. Tan, E. Memarzadeh, B. C. Oisen, and D. Mitlin, "Carbon nanosheet frameworks derived from peat moss as high performance sodium ion battery anodes," *ACS Nano*, vol. 7, no. 12, pp. 11004–11015, 2013.

[74] Y. Guo, W. Liu, R. Wu, L. Sun, Y. Zhang, Y. Cui, S. Liu, H. Wang, and B. Shan, "Marine-biomass-derived porous carbon sheets with a tunable N-doping content for superior sodium-ion storage," *ACS Applied Materials & Interfaces*, vol. 10, no. 44, pp. 38376–38386, 2018.

[75] Y. Chen, Y. Zhao, H. Liu, and T. Ma, "Crab Shell-Derived SnS_2/C and FeS_2/C carbon composites as anodes for high-performance sodium-ion batteries," *ACS Omega*, vol. 8, no. 10, pp. 9145–9153, 2023.

[76] B. Vinay, Y. Nikodimos, T. Agnihotri, S. A. Ahmed, T. M. Hagos, R. Hasan, E. B. Tamilarasan, W-N. Su, and B. J. Hwang, "Fluorine-free electrolytes in batteries: Principles, strategies, and advances," *Energy & Environmental Science*, vol. 18, no. 15, pp. 7326–7372, 2025.

[77] D. Qiu, W. Zhao, B. Zhang, M. T. Ahsan, Y. Wang, L. Zhang, X. Yang, and Y. Hou, "Ni-single atoms modification enabled kinetics enhanced and ultra-stable hard carbon anode for sodium-ion batteries,"*Advanced Energy Materials*, vol. 14, no. 20, p. 2400002, 2024.

[78] D. Qiu, Y. Wang, L. Zhang, H. Lei, H. Ying, J. Niu, M. Li, X. Yang, F. Wang, and R. Yang, "Regulating the oxygen-atom configuration of carbon anode enabling extremely fast-charging potassium-ion hybrid capacitors," *Nano Research*, vol. 18, no. 1, p. 94907033, 2025.

[79] S. Zheng, J. Zhang, H. Deng, Y. Du, and X. Shi, "Chitin derived nitrogen-doped porous carbons with ultrahigh specific surface area and tailored hierarchical porosity for high performance supercapacitors," *Journal of Bioresources and Bioproducts*, vol. 6, no. 2, pp. 142–151, 2021.

[80] T. Meenatchi, R. Subadevi, P. Kumar, S. Raghu, W. R. Liu, and M. Sivakumar, "An impact of sea sponge-derived hard carbon with the symbiosis of sodium ion battery and biomedical applications," *Journal of the Taiwan Institute of Chemical Engineers*, vol. 154, p. 105083, 2024.

[81] X. Meng, P. E. Savage, and D. Deng, "Trash to treasure: from harmful algal blooms to high-performance electrodes for sodium-ion batteries," *Environmental Science & Technology*, vol. 49, no. 20, pp. 12543–12550, 2015.

[82] L. Liu, Y. Tian, A. Abdussalam, M. R. H. S. Gilani, W. Zhang, and G. Xu, "Hard carbons as anodes in sodium-ion batteries: Sodium storage mechanism and optimization strategies," *Molecules*, vol. 27, no. 19, p. 6516, 2022.

[83] L. Liu, Y. Lan, N. Li, F. Sun, and N. Zhou, "Heterogeneous carbon coated resin-based hard carbon anode material for high-performance sodium ion batteries," *Materials Today Communications*, vol. 40, p. 109854, 2024.

[84] A. Björlin, A. Hansson, and L. Zhou, "Waste-derived hard carbon anode materials for sodium-ion batteries," *KTH Royal Institute of Technology*, pp. 1–57, 2023.

[85] Y. Xu, Y. Sun, L. Ma, J. Liu, C. Hai, D. Shengde, Q. Xu, X. He, and Z. Yuan, "Boosting sodium storage in hard carbon: A low-temperature ball milling approach for superior anode performance," *Langmuir*, vol. 41, no. 37, pp. 25546–25555, 2025.

[86] Q. Ma, Y. Wang, Z. Yi, L. Xe, F. Su, G. Sun, G. Hui, W. Xie, C. Chen, and Y. Hou, "Research on the controlled synthesis of phenolic resin-based carbon microspheres and their sodium storage behavior," *ChemistrySelect*, vol. 10, no. 16, pp. 1–11, 2025.

[87] A. Kamiyama, K. Kubota, T. Nakano, S. Fujimura, S. Shiraishi, H. Tsukada, and S. Komaba, "High-capacity hard carbon synthesized from macroporous phenolic resin for sodium-ion and potassium-ion battery," *ACS Applied Energy Materials*, vol. 3, no. 1, pp. 135–140, 2020.